Journal of Medicinal Chemistry

Article

pubs.acs.org/jmc

Synthesis and Evaluation of Novel Radioligands for Positron Emission Tomography Imaging of the Orexin-2 Receptor

Norihito Oi,[†,‡,§] Michiyuki Suzuki,[†,‡] Taro Terauchi,[†] Masaki Tokunaga,[‡] Yosuke Nakatani,[†,‡,§] Noboru Yamamoto,[†] Toshimitsu Fukumura,[‡] Ming-Rong Zhang,[‡] Tetsuya Suhara,[‡,§] and Makoto Higuchi*[,‡,§]

[†]Tsukuba Research Laboratories, Eisai Co., Ltd., 5-1-3 Tokodai, Tsukuba-shi, Ibaraki 300-2635, Japan;

[‡]Molecular Imaging Center, National Institute of Radiological Sciences, 4-9-1 Anagawa, Inage-ku, Chiba 263-8555, Japan;

[§]Graduate School of Medicine, Tohoku University, 1-1 Seiryo-machi, Aoba-ku, Sendai 980-8574, Japan

Supporting Information

ABSTRACT: Orexin receptors (OXRs) in the brain have been implicated in diverse physiological and neuropsychiatric conditions. Here we describe the design, synthesis, and evaluation of OXR ligands related to (1*R*,2*S*)-2-(((2-methyl-4-methoxymethylpyrimidin-5-yl)oxy)methyl)-*N*-(5-fluoropyridin-2-yl)-2-(3-fluorophenyl)cyclopropanecarboxamide (**9a**) applicable to positron emission tomography (PET) imaging. Structural features were incorporated to increase binding affinity for OXRs, to enable carbon-11 radiolabeling, and to adjust lipophilicity considered optimal for brain penetration and low nonspecific binding. **9a** displayed nanomolar affinity for OXRs, and autoradiography using rat brain sections showed that specific binding of [^{11}C]**9a** was distributed primarily to neocortical layer VI and hypothalamus, consistent with reported localizations of orexin-2 receptors (OX$_2$Rs). In vivo PET study of [^{11}C]**9a** demonstrated moderate uptake of radioactivity into rat and monkey brains under deficiency or blockade of P-glycoprotein, and distribution of PET signals in the brain was in agreement with autoradiographic data. Our approach and findings have provided significant information for development of OX$_2$R PET tracers.

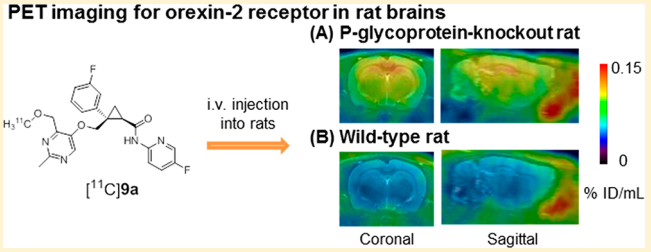

INTRODUCTION

Orexin or hypocretin receptors (OXRs) are G-protein-coupled receptors (GPCRs) that mediate the central actions of the endogenous neuropeptides orexin-A/hypocretin-1 (33 amino acid residues long) and orexin-B/hypocretin-2 (28 amino acid residues long) produced in the posterior and lateral hypothalamus.[1,2] Though synthesized by only a small population of neurons in the posterior and lateral hypothalamus, orexins exert multiple functions particularly in areas related to energy homeostasis, sleep/arousal, and brain reward mechanisms via signaling derived from orexin-1 receptor (OX$_1$R) and orexin-2 receptor (OX$_2$R) (also known as Hcrt1 and Hcrt2 receptors, respectively). Activation of orexin neurons contributes to the promotion of maintenance of wakefulness, and conversely, relative inactivity of orexin neurons induces the onset of sleep. Preclinical and clinical studies have revealed that the orexin pathway plays a critical role in motivation and sleep−wake regulation.[3,4] Abnormalities in orexin signaling have been observed in sleep disorders such as human narcolepsy−cataplexy syndrome,[5] irregularities in central vestibular motor control,[6] a variety of feeding and gastrointestinal disorders,[7,8] and addiction.[9] However, functional differences between signaling pathways derived from OX$_1$R and OX$_2$R have not been completely elucidated yet.

Due to the therapeutic potential of modulating these receptors, this has been an active area of research, primary for the treatment of insomnia.[10−15] Development of almorexant (**1**, a dual OX$_1$−OX$_2$R antagonist) from Actelion/GlaxoSmithKline was terminated at phase III clinical trial for the treatment of insomnia. SB-649868 (**2**, a dual OX$_1$−OX$_2$R antagonist) for sleep disorders had proceeded to phase II clinical development prior to **1**. Further advancement is exemplified by suvorexant (**3**).[16] a dual OX$_1$−OX$_2$R antagonist from Merck, and application of this new drug for the treatment of insomnia was filed for approval by United States Food and Drug Administration in 2012.

A suitable radioligand would help to examine the relationship between the therapeutic effect and receptor occupancy of this novel class of medicinal agents. A few tritiated tracers, such as [^{3}H]**1**,[17] [^{3}H]*N*-ethyl-2-[(6-methoxypyridin-3-yl)-(toluene-2-sulfonyl)amino]-*N*-pyridin-3-ylmethyl-1-acetamide ([^{3}H]EMPA, [^{3}H]**4**),[18] and [^{3}H]SB674042 ([^{3}H]**5**),[19] are known to be usable for in vitro analysis of OXRs.

Positron emission tomography (PET) is a useful tool for in vivo quantification of diverse biological processes, but only a

Received: January 30, 2013

dx.doi.org/10.1021/jm400772t | *J. Med. Chem.* XXXX, XXX, XXX−XXX

Scheme 1. Chemical Structures of Orexin Receptor Antagonists and Radioligands

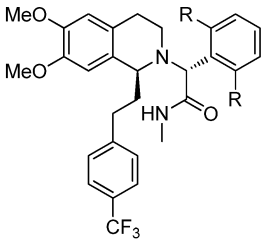

1: R = H (Almorexant, ACT-078573)
[^{3}H]**1**: R = T

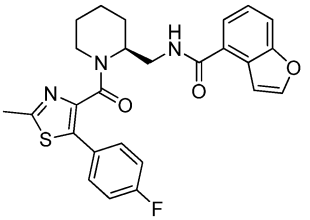

2 (SB-649868)

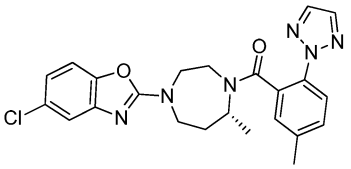

3 (Suvorexant, MK-4305)

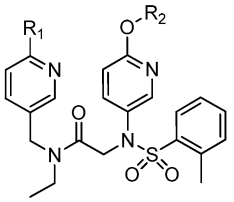

4: R_1 = H, R_2 = CH_3 (EMPA)
[^{3}H]**4**: R_1 = T, R_2 = CT_3
[^{11}C]**4**: R_1 = H, R_2 = $^{11}CH_3$

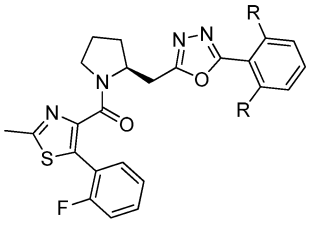

5: R = H (SB-674042)
[^{3}H]**5**: R = T

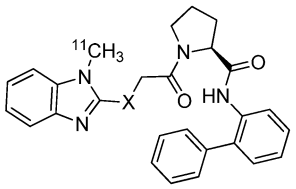

[^{11}C]**6a**: X = S ([^{11}C]BBAC)
[^{11}C]**6b**: X = CH_2 ([^{11}C]BBPC)

Scheme 2. Chemical Structures of PET Tracer Candidates and Their ^{11}C-Labeling Versions

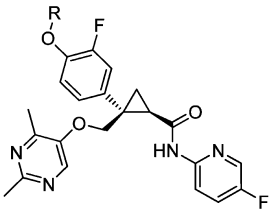

7a: R = CH_3
[^{11}C]**7a**: R = $^{11}CH_3$

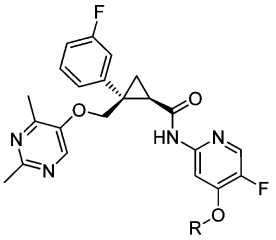

8a: R = CH_3
[^{11}C]**8a**: R = $^{11}CH_3$

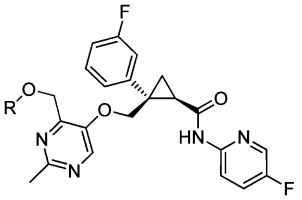

9a: R = CH_3
[^{11}C]**9a**: R = $^{11}CH_3$

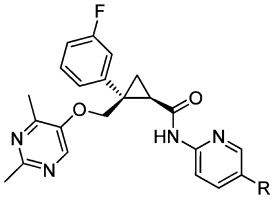

10a: R = CN
[^{11}C]**10a**: R = ^{11}CN

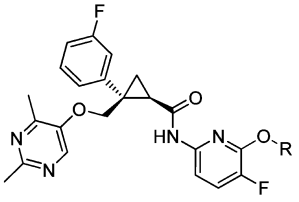

11a: R = CH_3
[^{11}C]**11a**: R = $^{11}CH_3$

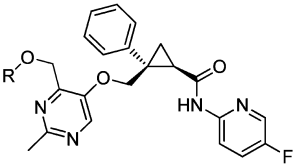

12a: R = CH_3
[^{11}C]**12a**: R = $^{11}CH_3$

small number of PET tracers, including [^{11}C]BBAC ([^{11}C]**6a**),[20] [^{11}C]BBPC ([^{11}C]**6b**),[20] and [^{11}C]**4**,[21] have been evaluated for imaging of OXRs. However, in vivo PET studies of [^{11}C]**6a** and [^{11}C]**6b** did not demonstrate the uptake of this radioligand into the brain of rhesus monkeys.[20] [^{11}C]**4** also showed very low uptake into the brain of a baboon as measured with PET.[21] Hence, a novel PET tracer for OXRs would be useful to understand the relationships between dose and receptor occupancy, efficacy, and adverse events of therapeutic agents, to better guide the appropriate dose setting in clinical trials. Additionally, receptor occupancy could be used as an objective outcome measure in a therapeutic assessment. This would particularly serve evaluation of drugs for diseases in which functional biomarkers such as polysomnography (in case of insomnia) are unavailable.

It has been documented that mRNAs encoding OX_1R and OX_2R are expressed in several distinct regions of the rat brain.[22,23] High structural and functional homology is also reported for rat and human OX_1R and OX_2R, and orexins are well conserved across mammalian species.[24] It is of particular interest to target either OX_1R or OX_2R by synergistically using therapeutic and imaging agents. OX_2R is present with a relatively high density in the hippocampal CA3 region, neocortical layer VI, tuberomammilliary nucleus, induseum

dx.doi.org/10.1021/jm400772t | J. Med. Chem. XXXX, XXX, XXX−XXX

Table 1. Pharmacological Properties of PET Tracer Candidates

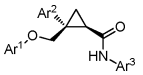

compound	Ar^1	Ar^2	Ar^3	*in vitro* binding affinity OX$_2$ Ki (nM)	*in vitro* binding affinity OX$_1$ Ki (nM)	lipophilicity cLogP[a]	lipophilicity log *D*[b]	corrected P-gp FR[c] (MDR1 FR / PK1 FR)
7a				7	30	3.85	3.32	1.55 (1.24/0.80)
8a				2	3	4.18	2.93	2.06 (2.45/1.19)
9a				1	1	3.29	2.97	3.11 (2.61/0.84)
10a				5	32	3.43	*d*	1.76 (1.92/1.09)
11a				2	12	4.58	3.60	1.21 (0.98/0.81)
12a				1	9	3.15	*d*	2.03 (1.97/0.97)

[a]cLogP value was calculated by Daylight Software ver. 4.94 (Daylight Chemical Information Systems, Inc., Niguel, CA). [b]Log *D* values were quantified in *n*-octanol/phosphate buffer (pH 7.4) by the shake-flask method (n = 3; maximum range, ±5%). [c]See P-gp Transcellular Transport Study in Experimental Section. [d]Not determined.

griseum, medial thalamic areas, and nucleus accumbens, in distinction from abundant localization of OX$_1$R to the prefrontal cortex, hippocampus, paraventricular thalamic nucleus, ventromedial hypothalamic nucleus, dorsal raphe nucleus, and locus coeruleus.[23] This is consistent with reported distribution of in vitro autoradiographic labeling with [^{3}H]**4**,[18] which is selective for OX$_2$R, and supports the notion that specific binding of a PET ligand to the neocortex (particularly layer VI) could be an indicator of its reactivity with OX$_2$R.

We have attempted to identify suitable PET tracer candidates for OXRs among cyclopropane derivatives, one of our novel classes of compounds with relatively highly binding affinity for OX$_2$R than for OX$_1$R.[25] We have selected several cyclopropane analogs **7a**−**12a** (Scheme 2) as PET tracer candidates for OX$_2$R imaging based on their binding affinity, lipophilicity, and flux ratio (FR) for efflux transporter to maximize their ability to penetrate the blood−brain barrier (BBB) and overall feasibility of radiolabeling.

We report here a systematic strategy for discovering suitable radioligands that can be used as PET tracers for imaging of OX$_2$R in the central nervous system (CNS). First, we calculated the maximal number of binding sites (B_{max}) for OX$_2$R in the brain and estimated the affinity of a compound required for PET imaging on the basis of this B_{max} value. A set of compounds were then selected in consideration of these affinity data along with FR values. We also conducted radiosynthesis and in vivo evaluation of these compounds in rats and a monkey and found that [^{11}C]**9a** may have potential as a lead for further development of PET tracer candidates.

RESULTS AND DISCUSSION

Selection of PET Tracer Candidates. One hundred and thirty compounds with potent binding affinity (inhibition constant K_i < 10 nM) for OX$_2$R were selected as initial PET tracer candidates. The lipophilicity of this series of compounds was relatively high with cLogP values ranging from 2.4 to 5.6 (cLogP values; 4.12 ± 0.65, mean ± SD), and compounds with cLogP > 4.7 were not taken into consideration. We also looked at corrected FR calculated between LLC-PK1 cells and multidrug resistance protein 1 (MDR1) expressed in LLC-PK1 cells (LLC-MDR1) to narrow down our list of candidate compounds likely to penetrate BBB, because corrected FR was demonstrated to be well correlated to and thus highly predictive of in vivo function of P-glycoprotein (P-gp) located on cerebral endothelial cells.[26] Therefore, compounds with FR around 3.0 or below were selected. Consequently, 74 compounds met our criteria. Several compounds were then chosen as for PET tracer candidates based on their affinity and suitable characteristics as described below.

While assessing these candidates, we evaluated the density of OX$_2$R in layer VI of the neocortex in the rat brain and calculated B_{max} for [^{3}H]**4** was 6.5 nM (see Experimental Section). Because the binding potential for a ligand depends on the ratio between B_{max} and dissociation constant (K_d, in this context equivalent to inhibition constant, K_i), we prioritized the K_i value.[27−30] High priority was given to the affinity for OX$_2$R over selectivity for OX$_2$R versus OX$_1$R, because these two receptor subtypes were assumed to be distinguishable by their distinct localizations in imaging assays. Six compounds, which have K_i values equivalent to or smaller than B_{max}, displayed

dx.doi.org/10.1021/jm400772t | J. Med. Chem. XXXX, XXX, XXX−XXX

Scheme 3. Syntheses of Common Intermediate 18[a]

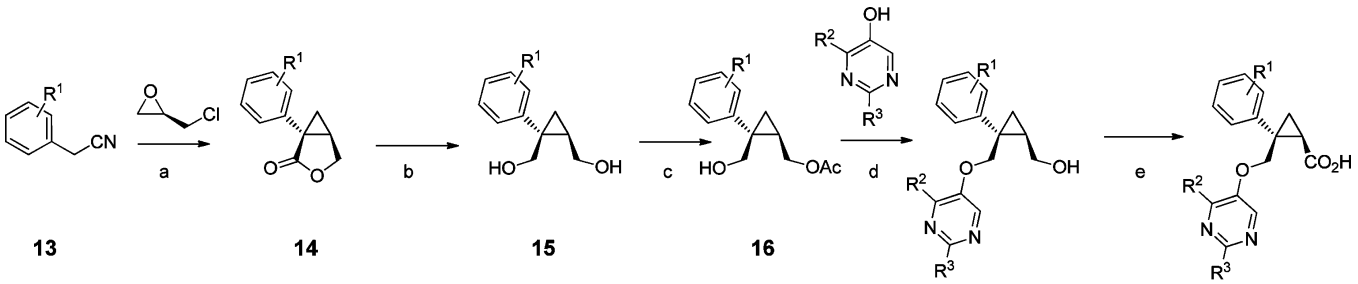

	R^1	R^2	R^3
a	3-F	MOM	Me
b	3-F	Me	Me
c	3-F, 4-MOMO	Me	Me
d	H	Me	Me
e	H	MOM	Me

[a]Reagents and conditions: (a) NaHMDS, THF, 0 °C, 3 h, then KOH, EtOH, reflux, 8 h, then HCl, 0 °C–rt, 3 h; (b) $NaBH_4$, MeOH–THF, 0 °C–rt, 1 h; (c) Novozym 435, vinyl acetate, rt, 17 h; (d) DIAD, PPh_3, 0 °C–rt, 15 h, then NaOH, EtOH–H_2O, rt, 1 h; (e) $(COCl)_2$, DMSO, TEA, DCM, −60 °C–rt, 1 h, then 2-methyl-2-butene, $NaClO_2$, NaH_2PO_4, acetone–H_2O, rt, 14 h.

favorable properties by meeting most of our requirements as listed in Table 1. We thereafter radiolabeled all six compounds for subsequent autoradiographic characterization to validate the usefulness of selecting these criteria when screening for an imaging agent.

Chemistry.[25] Preparation for all common key intermediates, carboxylic acids **18a–e**, is summarized in Scheme 3. The novel unlabeled compounds **7a–12a** were synthesized according to reaction sequences delineated in Scheme 4. Cyclopropane ring formation was carried out by the reaction of an appropriate phenyl acetonitrile **13** with (*R*)-(−)-epichlorohydrin to give lactone **14**.[31] Reduction of lactone **14** with sodium borohydride readily gave corresponding diol **15**, which could be regioselectively acetylated at the 2-methanol position by Novozyme (lipase acrylic resin from *Candida antarctica*), to give the desired monoacetylated compound **16**. Mitsunobu reaction of the corresponding alcohol with various kinds of hydroxyl pyrimidines led to the production of **17** as an intermediate. Hydrolysis of **17** with sodium hydroxide (NaOH), followed by treatment with an appropriate oxidizer, afforded corresponding carboxylic acid **18**.

All of the selected PET tracer candidates **7a–12a** were prepared in an unlabeled form. Also, the corresponding precursors **7b–12b** for radiosynthesis were prepared, as shown in Scheme 4. Condensation of **18** with various kinds of pyridines to form an amide bond was carried out via the amidation of carboxylic acid with aminopyridines or palladium coupling of carboxamide and chloropyridines.

For candidates with a methoxy group, we prepared corresponding hydroxy derivative as a radiolabeling precursor. **8b** and **11b** were prepared from target molecule **8a** and **11a**, respectively, by cleavage of the methoxy group with pyridine hydrochloride. To prepare **7a** and its precursor **7b**, methoxymethyl (MOM) group was introduced prior to the first step. To prepare precursors of **9a** and **12a**, a methanol moiety on the pyrimidine ring was required. Therefore, hydroxy precursors, **9c** and **12c** were converted to **9b** and **12b**, respectively, in three steps via bromination of side chain by using $Br_2/CHCl_3$; note that the reaction mainly gave 4-bromination with a trace amount of 2,4-dibromide. Subsequent substitution for the acetoxy group with sodium acetate followed by hydrolysis produced **9b** and **12b**. Moreover, **10a** and its precursor **10b** could be prepared by reacting the common starting material **18b** with 2-amino-5-iodopyridine and 2-amino-5-cyanopyridine, respectively.

Radiosynthesis. Radiosynthesis of [^{11}C]**7a–12a** was performed using a handmade automated synthesis system equipped with two units for [^{11}C]methylation and [^{11}C]-cyanation. The *O*-[^{11}C]methyl ligands [^{11}C]**7a**, [^{11}C]**8a**, [^{11}C]**9a**, [^{11}C]**11a**, and [^{11}C]**12a** were prepared by reacting precursor **7b**, **8b**, **9b**, **11b**, and **12b** with [^{11}C]methyl iodide ([^{11}C]CH_3I), respectively, with specific activity of 37–185 GBq/μmol (Scheme 5). [^{11}C]CH_3I was prepared by reducing cyclotron-produced [^{11}C]CO_2 with $LiAlH_4$, followed by iodination with 57% hydroiodic acid.[32] For generation of radiolabeled **7a**, **8a**, **9a**, **11a**, and **12a**, [^{11}C]CH_3I was trapped in a *N*,*N*-dimethylformamide (DMF) solution of precursors **7b**, **8b**, **9b**, **11b**, and **12b**, respectively, with an appropriate amount of base at −15 °C. For example, [^{11}C]methylation of **9b** with [^{11}C]CH_3I under treatment with NaH proceeded efficiently for 3 min at 40 °C. Semipreparative HPLC purification for the reaction mixtures gave [^{11}C]**9a** with 26 ± 4% (n = 5) radiochemical yields (decay-corrected) based on [^{11}C]CO_2 (Supporting Information: Figure 4). [^{11}C]**12a** was obtained from **12b** in the same manner. [^{11}C]**7a**, [^{11}C]**8a**, and [^{11}C]**11a** were prepared from their precursors, **7b**, **8b**, and **11b**,

dx.doi.org/10.1021/jm400772t | J. Med. Chem. XXXX, XXX, XXX–XXX

Scheme 4. Syntheses of 7a−12a and Their Radiolabeling Precursors 7b−12b[a]

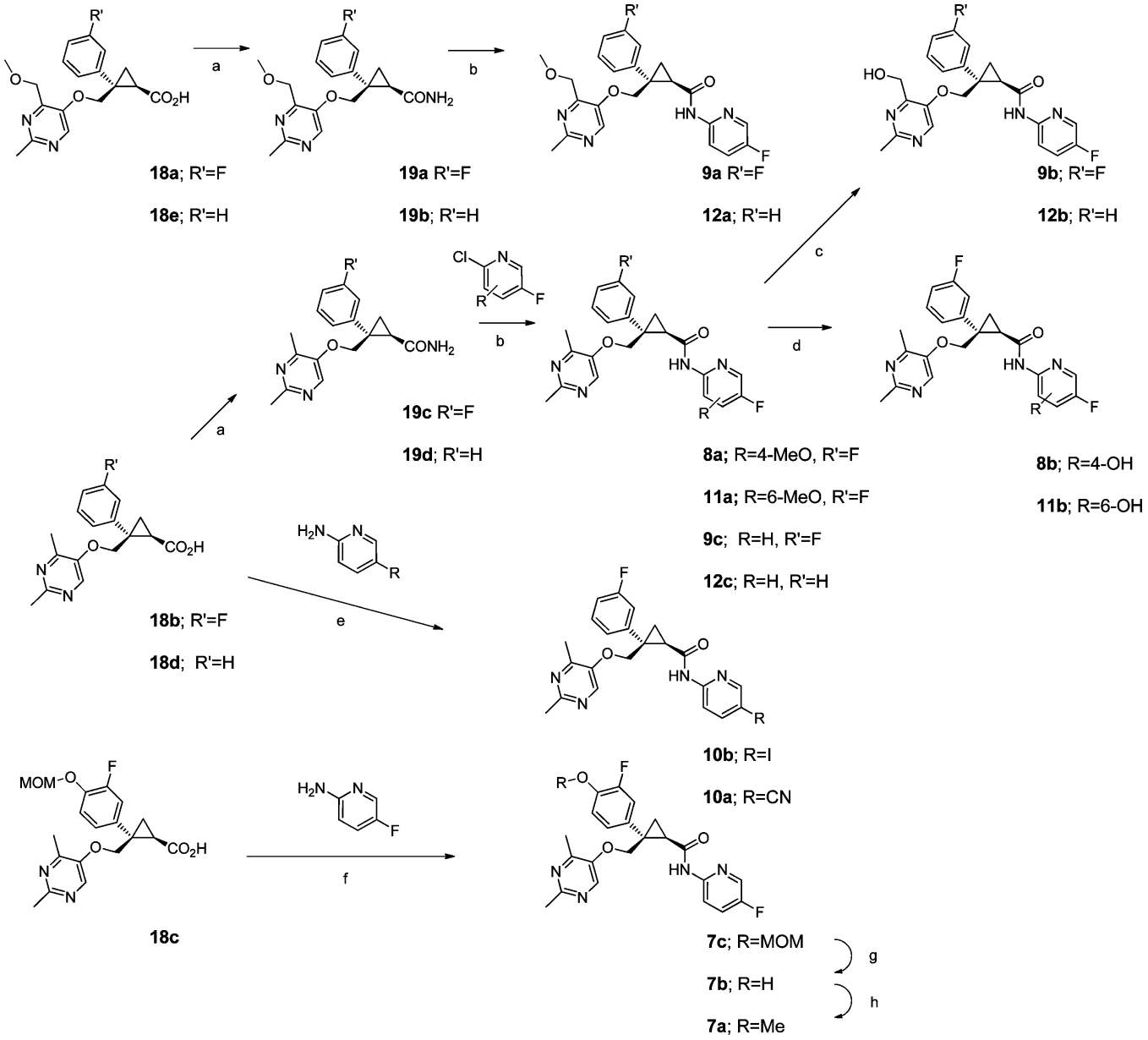

[a]Reagents and conditions: (a) WSC, HOBt, NH_4Cl, DIPEA, DMF, rt, 7 days; (b) 2-chloro-5-fluoropyridine, K_3PO_4, Xant phos, $Pd_2(dba)_3$, dioxane, 80 °C, 1 day; (c) i: Br_2, $CHCl_3$, 0 °C−rt, 4 days; ii: AcONa, DMF, 50 °C, 2 h; iii: 1 M NaOH, MeOH, rt, 1.5 h, (d) pyridine−HCl salt, 120 °C, 2 h; (e) i: $(COCl)_2$, DMF, DCM, rt, 1 h; ii; DIPEA, 2-aminopyridines, THF, 60 °C, 1 h; (f) 2-amino-5-fluoropyridines, HATU, DIPEA, DMF, 0 °C−rt, 3 h; (g) 5 M HCl, THF, rt, 2 h; (h) CH_3I, Cs_2CO_3, DMF, rt, 2 h.

respectively, according to the procedure described for the synthesis of [^{11}C]**9a** using K_2CO_3 instead of NaH. In the case of [^{11}C]**10a**, we performed [^{11}C]cyanation of **10b** to obtain [^{11}C]**10a**, because both **10a** and **10b** could be readily prepared in one step from their common precursor **18b**.

The identities of [^{11}C]**7a−12a** were confirmed by coinjection with the corresponding unlabeled **7a−12a** on reverse phased−analytical HPLC. In the final product solutions, their radiochemical purities were higher than 99%. Additionally, specific activity of each product was calculated from the UV absorption area at 254 nm based on standard curves from known concentrations of unlabeled samples in common ratio. The amount of carrier in the final product solution was measured by the same analytical HPLC. Moreover, these radioligands did not show radiolysis at room temperature (rt) for 90 min after formulation, indicating radiochemical stability over the period of at least one PET scan.

In Vitro Autoradiography Study. Figure 1 shows representative in vitro autoradiographic images of coronal rat brain sections with all labeled compounds examined. Among these radioligands, only [^{11}C]**8a** and [^{11}C]**9a** exhibited detectable specific binding to OX_2R in layer VI (red arrowhead) of the neocortex and hypothalamus, in line with known distribution of OX_2R, and [^{11}C]**9a** showed the highest contrast between total (Figure 1E) and nonspecific binding (Figure 1F) of all tested compounds. Moreover, the localizations of [^{11}C]**8a** and [^{11}C]**9a** signals were very similar to that of [^{3}H]**4** (Figure 1M, 1N).[18] As for the current series of

dx.doi.org/10.1021/jm400772t | J. Med. Chem. XXXX, XXX, XXX−XXX

Scheme 5. Radiosynthesis of [^{11}C]7a−12a[a]

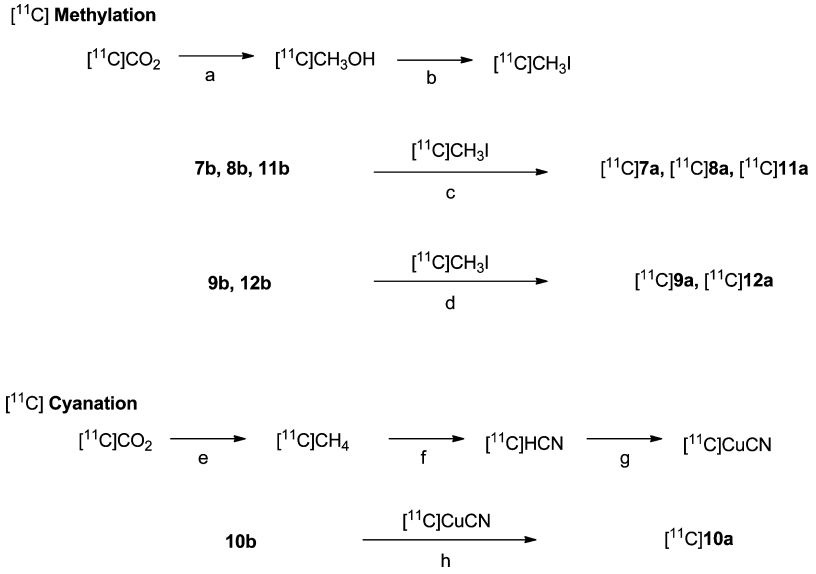

[a]Reagents and conditions: (a) $LiAlH_4$, THF, −15 °C, 2 min; (b) hydroiodic acid, 180 °C, 2 min; (c) K_2CO_3, DMF, 50 °C, 3 min; (d) NaH, DMF, 40 °C, 3 min; (e) H_2, Ni, 400 °C; (f) NH_3, Pt, 960 °C; (g) $Na_2S_2O_5$, $CuSO_4$, H_2O, 80 °C, 2 min; (h) DMF, 165 °C, 5 min.

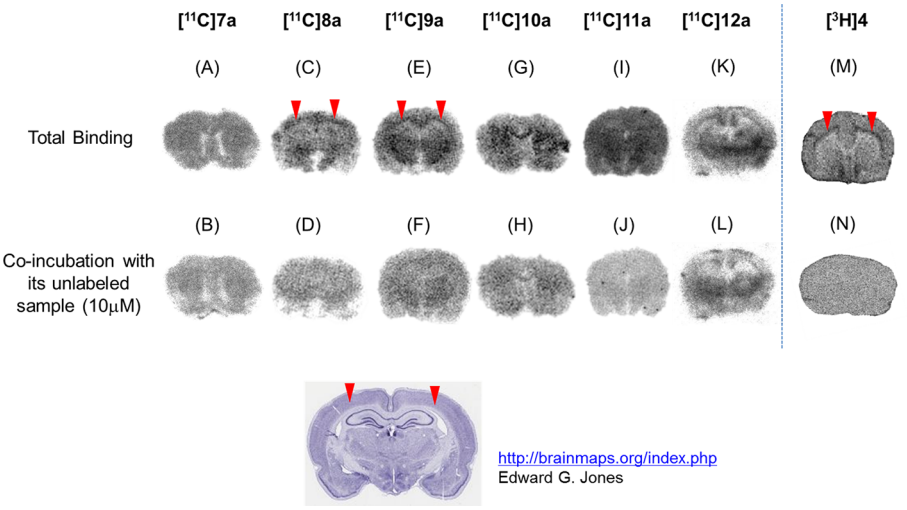

Figure 1. Representative in vitro autoradiographic images of rat brains. Representative in vitro autoradiographic images of rat brains treated with [^{11}C]**7a** (7.6 nM, A, B), [^{11}C]**8a** (2.0 nM, C, D), [^{11}C]**9a** (2.5 nM, E, F), [^{11}C]**10a** (59.0 nM, G, H), [^{11}C]**11a** (1.6 nM, I, J), [^{11}C]**12a** (2.6 nM, K, L), [^{3}H]**4** (5.0 nM, M, N). All coronal slices were collected about −4 mm from bregma. (A) [^{11}C]**7a** only; (B) [^{11}C]**7a** with **7a** (10 μM); (C) [^{11}C]**8a** only; (D) [^{11}C]**8a** with **8a** (10 μM); (E) [^{11}C]**9a** only; (F) [^{11}C]**9a** with **9a** (10 μM); (G) [^{11}C]**10a** only; (H) [^{11}C]**10a** with **10a** (10 μM); (I) [^{11}C]**11a** only; (J) [^{11}C]**11a** with **11a** (10 μM); (K) [^{11}C]**12a** only; (L) [^{11}C]**12a** with **12a** (10 μM); (M) [^{3}H]**4** only; (N) [^{3}H]**4** with **4** (10 μM).

compounds, autoradiography results indicate that [^{11}C]**9a** is featured by high affinity and relatively low nonspecific binding related as predicted by cLogP values. By contrast, [^{11}C]**7a**, [^{11}C]**10a**, and [^{11}C]**11a** did not produce signals reflecting the distribution of OX_2R. Despite the K_i values for [^{11}C]**11a** comparable to that of [^{11}C]**9a** (Table 1), this radioligand homogeneously bound to the brain slices presumably due to its higher lipophilicity relative to [^{11}C]**9a**. To clarify the relationship between lipophilicity of the compounds and their performance in autoradiographic imaging, we quantified log *D* values of selected chemicals using *n*-octanol and phosphate buffer (Table 1). The log *D* value of [^{11}C]**8a** (2.93) was comparable to [^{11}C]**9a** (2.97), and both radioligands were capable of producing autoradiographic signals consistent with OX_2R. Meanwhile, the log *D* value of [^{11}C]**11a** (3.60) was higher than those of [^{11}C]**8a** and [^{11}C]**9a**, presumably accounting for homogeneous binding of this compound to the brain slices. Hence, the log *D* value may serve as an informative index in search for appropriate imaging agents. Failure of staining OX_2R with [^{11}C]**7a** and [^{11}C]**10a** with a larger K_i than [^{11}C]**8a** and [^{11}C]**9a** indicates that K_i values far below B_{max} are required for high-contrast imaging of OX_2R (see Receptor Binding Assay for B_{max} Evaluation in Experimental Section).

Specificity of Autoradiographic Labeling with [^{11}C]9a for OX_2R versus OX_1R. To clarify specificity of [^{11}C]**9a** signals in the neocortex for OX_2R versus OX_1R and other binding elements, in vitro autoradiographic assays were performed for rat brain sections under conditions with **3** (OX_1R and OX_2R dual antagonist) and **4** (OX_2R-selective

dx.doi.org/10.1021/jm400772t | J. Med. Chem. XXXX, XXX, XXX−XXX

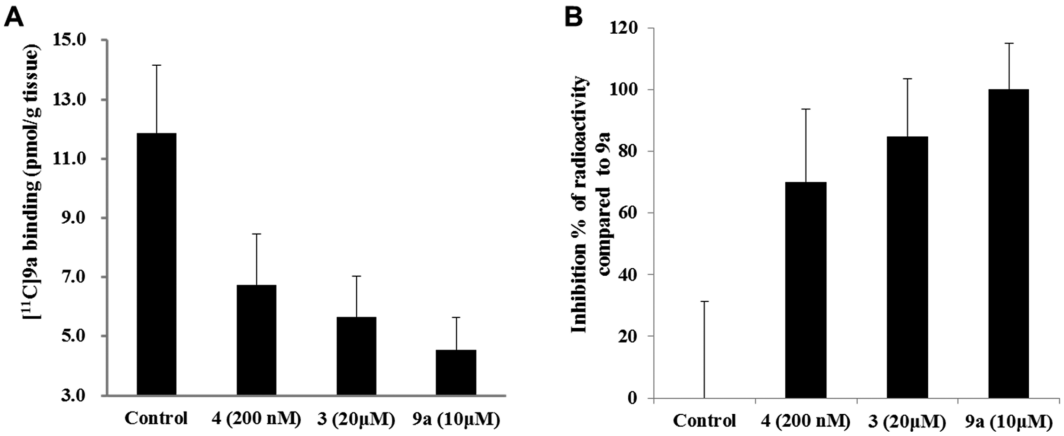

Figure 2. In vitro autoradiographic binding of [^{11}C]**9a** to the rat neocortex in the absence (control) and presence of nonradioactive OXR ligands. (A) Total binding of [^{11}C]**9a** (3.6 nM) to the cortical layer VI at baseline and in coincubation with **4** (200 nM), **3** (20 μM), and unlabeled **9a** (10 μM). (B) Inhibition of specific radioligand binding as percentage of inhibition by 10 μM unlabeled **9a**. We conceived that a decrease of total [^{11}C]**9a** binding in the presence of 10 μM unlabeled **9a** corresponds to the full abolishment of specific [^{11}C]**9a** binding, and reduction of total binding in each condition was normalized by this full abolishment to determine inhibition of specific radioligand binding.

antagonist). Specific binding of [^{11}C]**9a** in the neocortical layer VI was decreased by 85% in the presence of 20 μM **3** (Figure 2), suggesting that specific binding sites for [^{11}C]**9a** are primarily composed of OXRs. Addition of 200 nM **4** to the reaction also diminished specific radioligand binding by 70%, and we accordingly conceived that OX_2R was a major specific binding component for [^{11}C]**9a** in the neocortex.

Activity of 9a on Off-Target Binding Components. Pharmacological profile of **9a** was further investigated by GPCR panel assays. **9a** (10 μM) was inactive on representative 24 off-target GPCRs, except its weak and modest antagonistic activity on cannabinoid CB_1 and melatonin MT_1 receptors, respectively (Table 2 in Supporting Information). In consideration of the concentration of **9a** reacted here, it is unlikely that a significant portion of [^{11}C]**9a** at much lower concentrations in autoradiographic and PET experiments reacted with CB_1. In addition, distribution of MT_1[33] is distinct from that of OXRs, and therefore autoradiographic binding of [^{11}C]**9a** to MT_1 in the neocortex is presumed to be negligible.

These data are consistent with autoradiographic observations indicating that specific binding of [^{11}C]**9a** is attributable to its interaction with OX_2R, although the possibility that **9a** binds to GPCRs and non-GPCR components unexamined here could not be ruled out. On the basis of these in vitro results, we further evaluated [^{11}C]**8a** and [^{11}C]**9a** using in vivo PET imaging.

In Vivo PET Studies in Rats. PET scans were conducted using [^{11}C]**9a**, because it produced the clearest contrast in autoradiography imaging. Meanwhile, in vitro assay indicated that **9a** exhibited FR larger than that of the other selected compounds (Table 1), and therefore P-gp-knockout rats were used for the PET scan in addition to wild-type rats. Notable retention of radioactivity in OX_2R-rich brain regions in contrast with its low uptake in the cerebellum, which lacks the receptors, was observed in P-gp-knockout rats (n = 3) (Figure 3A,C). However, differences in the radioligand retention in the neocortex, hippocampus, and thalamus could not be demonstrated clearly. Additionally, there was only minimal uptake of radioactivity into the brains of wild-type rats (n = 3) (Figure 3B,D). To further examine the specificity and displaceability of [^{11}C]**9a** binding in P-gp-knockout rats, a PET scan was conducted 1 h after oral administration of 10 mg/kg of unlabeled **9a**, because pharmacological effects of orally administrated **9a** at this dose were clearly demonstrated in our spontaneous locomotion and sleep efficacy tests for wild-type mice. As shown on the time−radioactivity curves (Figure 3E), pretreatment with unlabeled **9a** markedly reduced the radioactivity compared to control (Figure 3C). Radioligand retention was significantly inhibited in all brain regions except the cerebellum, and the distribution of radioactivity became fairly uniform throughout the brain. This resulted in a decrease in target-to-cerebellum ratios of radioactivity by the blockade (Figure 3F), supporting the in vivo imaging of [^{11}C]**9a** with its specific and saturable binding sites in the brain.

Additional PET scans were conducted using [^{11}C]**8a** in P-gp-knockout rat and wild-type rat, respectively. Overall, [^{11}C]**8a** showed time−radioactivity curves similar to that of [^{11}C]**9a**, but there was however relatively lower retention compared with that for [^{11}C]**9a** (see Supporting Information, Figure 5).

Ex Vivo Metabolite Study in a P-gp-knockout Rat. An ex vivo metabolite study was performed by using P-gp-knockout rat (identical to one of the individuals used for PET study), and we identified a radiometabolite which was more hydrophilic than the parent tracer in plasma and brain. Retention times (t_Rs) for this metabolite and parent compound were 2.0 and 5.2 min, respectively. More than half of radioactivity in the brain was derived from the parent tracer at 30 min postinjection, while less unchanged [^{11}C]**9a** remained in plasma (Table 2). These data indicate that in vivo PET signals in the brains of P-gp-knockout rats (Figure 3A,C) were composed of [^{11}C]**9a** and its metabolite.

In Vivo PET Study in Rhesus Monkey. The uptake of radioactivity in all brain regions peaked at 30 s after intravenous [^{11}C]**9a** injection (Figure 4A,B), followed by a rapid decline of radioactivity and low level retention in the brain (Figure 4B), suggesting that radioactivity was rapidly cleared from the brain by P-gp transporter in the initial phase of the scan. To examine this notion, an additional PET scan with [^{11}C]**9a** was conducted under blockade of P-gp transporter. The monkey used for the baseline PET assay underwent a [^{11}C]**9a**-PET measurement (Figure 4C,D), which was initiated at 0.25 h after intravenous administration of tariquidar (XR9576, 8 mg/kg).[34] Pretreatment with tariquidar markedly increased the uptake of radioactivity into the brain compared to the baseline data.

dx.doi.org/10.1021/jm400772t | J. Med. Chem. XXXX, XXX, XXX−XXX

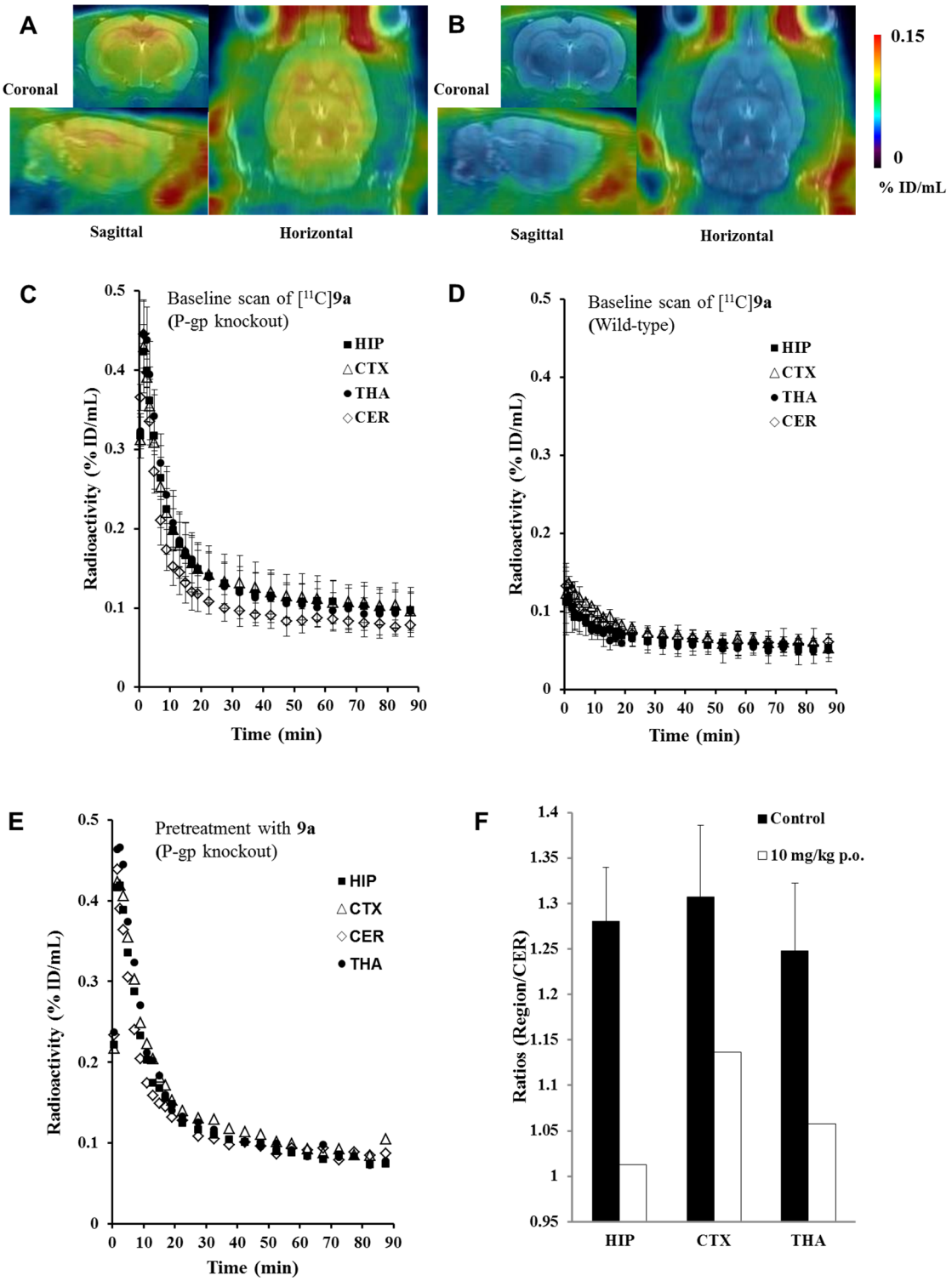

Figure 3. Rat PET study of [^{11}C]**9a**. (A, B) Representative PET images of P-gp-knockout (A) and wild-type (B) rat brains generated by averaging dynamic data at 0−90 min after intravenous injection of [^{11}C]**9a**. PET images are superimposed on a magnetic resonance imaging (MRI) template. (C, D) Time−radioactivity curves for [^{11}C]**9a** in the neocortex (CTX), hippocampus (HIP), thalamus (THA), and cerebellum (CER) of P-gp-knockout (C) and wild-type (D) rat brains (triplicated experiments). (E) Time−radioactivity curves for [^{11}C]**9** in the medial prefrontal cortex (MPFC), HIP, CTX, and CER of P-gp-knockout rat brains after blockade with **9a** (10 mg/kg po, 1 h before radioligand injection). (F) Target-to-cerebellum ratio of AUC in the P-gp-knockout rat brain in control (closed bars) and blockade (open bars) experiments. The radioactivity is expressed as percentage of injected radioligand dose per unit volume of tissue (% ID/mL).

Similar to in vivo PET data in P-gp-knockout rats (Figure 3C), radioactivity retention was the highest in the neocortex, implying that PET signals in the brain of the tariquidar-treated monkey may reflect distribution of OX_2R. As indicated by autoradiography and PET results, [^{11}C]**9a** had affinity for OX_2R sufficient for in vivo PET imaging, but its poor BBB permeability and rapid clearance from the brain did not allow us to sensitively detect OXRs except for the brains of animals

dx.doi.org/10.1021/jm400772t | J. Med. Chem. XXXX, XXX, XXX−XXX

Table 2. Fraction of Unchanged [^{11}C]9a as Percentage of Total Radioactivity in P-gp-knockout Rat Plasma and Brain

	fraction of unmetabolized compound in P-gp-knockout rat tissues (%) (n = 1)	
time after injection (min)	brain	plasma
30	54	12

deficient in P-gp or treated with a P-gp inhibitor, highlighting the significance of FR values for efflux transporters.

CONCLUSIONS

We developed a novel series of cyclopropane derivatives that potentially set the path for the development of future potent PET imaging tracers for OXRs. Based on affinity ($K_i \leq B_{max}$ = 6.5 nM), lipophilicity (2.4 < cLogP < 4.7), and efflux properties of the P-gp transporter (FR ≤ 3), we selected and radiolabeled

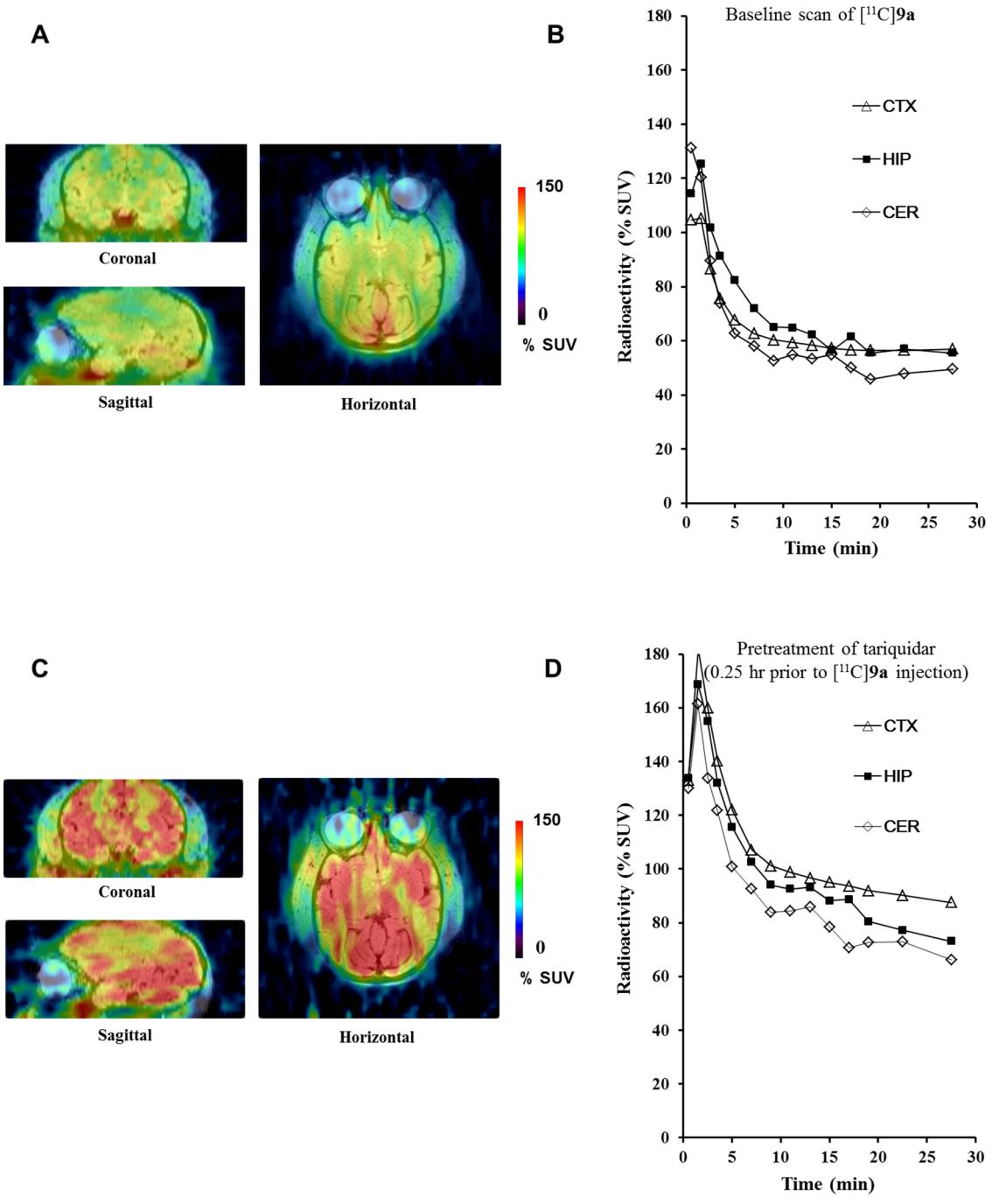

Figure 4. Rhesus monkey PET study of [^{11}C]**9a**. (A, C) Orthogonal PET images of rhesus monkey brain generated by averaging dynamic scan data at 0−90 min after intravenous injection of [^{11}C]**9a**. Orthogonal images at baseline (A) and under blockade of P-gp by pretreatment with tariquidar (8 mg/kg) at 0.25 h before radioligand injection (C) are superimposed on individual MRI data. (B, D) Time−radioactivity curves for [^{11}C]**9a** in the CTX, HIP, and CER of a rhesus monkey at baseline (B) and under P-gp blockade (D). Radioactivity is expressed as percentage of standardized uptake value (% SUV).

dx.doi.org/10.1021/jm400772t | J. Med. Chem. XXXX, XXX, XXX−XXX

several compounds as PET tracer candidates. Among them, [^{11}C]**9a** showed specific binding for OXRs indicated by both in vitro autoradiography of rat brain slices and in vivo PET imaging of P-gp-knockout rats, along with the blockade of radioligand binding by unlabeled compounds and insignificant reactivity with GPCRs other than OXRs. The B_{max} value for the receptors obtained from in vitro binding assays enabled us to estimate correctly the affinity of a ligand required for producing a sufficient imaging contrast, and also the lipophilicity (measured as log D value) of the compounds had an impact on the performance of the radioligands in the autoradiographic imaging well. According to the autoradiographic data of [^{11}C]**8a** and [^{11}C]**9a** (Figure 1C, 1E), a compound with a B_{max}/K_i ratio of 5.0 or higher seems to be required for a PET tracer candidate to detect specific binding to OX_2R.[28−30] By characterizing the binding profile of **9a**, it has potential to visualize neocortical OX_2R with adequate specificity (Figure 2). For in vivo visualization of OX_2R in the brain, the permeability into the CNS, which could be estimated by FR and lipophilicity, was equally important (Figures 3 and 4). Moreover, robust metabolic stability is required for further improvement (Table 2). We could not identify a PET tracer that can be used to clearly visualize OX_2R in wild-type rat and nonhuman primate. However, we succeeded in clarifying the preferred profile for an OX_2R PET tracer. Hence, our approach and findings have provided substantial insights into the development of next-generation OX_2R PET tracers.

EXPERIMENTAL SECTION

1. Materials and Methods. Melting points were measured using a micro melting point apparatus (MP-500P; Yanaco, Tokyo, Japan) and are uncorrected. ^{1}H NMR spectra were recorded on a JEOL-AL-300 spectrometer (operating at 300 MHz, JEOL, Tokyo, Japan) or Varian Mercury 400 spectrometer (operating at 400 MHz, Varian, Palo Alto, CA) or Bruker Avance 600 spectrometer (operating at 600 MHz, Bruker BioSpin, Ettlingen, Germany), with tetramethylsilane as an internal standard. All chemical shifts (δ) were reported in parts per million (ppm) downfield relative to the chemical shift of tetramethylsilane. Signals are quoted as s (singlet), d (doublet), dt (double triplet), t (triplet), q (quartet), or m (multiplet). Fast atom bombardment mass spectra (FAB−MS) and high-resolution mass spectra (HRMS) were obtained on a JEOL-AL-300 spectrometer (JEOL) and recorded on the spectrometer. Electrospray ionization mass spectra (ESI-MS) were recorded on ThermoFisherScientific LTQ-Orbitrap XL spectrometer (ThermoFisherScientific Inc., Waltham, MA). Column chromatography was performed using Fuji Silysia BW-300 (300 mesh). Reverse phase HPLC was performed using a JASCO HPLC module (JASCO, Tokyo, Japan) equipped with YMC Pack Pro C_{18} columns (S-5 μm, 10 mm ID × 250 mm, YMC, Kyoto, Japan) utilizing a 0.1% triethylamine (TEA) in water/methanol or 0.1% TEA in water/acetonitrile (MeCN) for semiseparative purification. Chemical purity analysis was carried out by using YMC Pack Pro C_{18} columns (S-5 μm, 4.6 mm ID × 150 mm, YMC) with UV detector at 254 nm. Under radio-HPLC purification and analysis, an effluent of radio activity was monitored by using a NaI (Tl) scintillation detector system. All chemical reagents and solvents were purchased from commercial sources (Sigma-Aldrich, St. Louis, MO; Wako Pure Chemical Industries, Osaka, Japan; Tokyo Chemical Industries, Tokyo, Japan) and used as supplied. [^{3}H]**4** was synthesized in PerkinElmer Life & Analytical Sciences (Waltham, MA). Tariquidar was purchased from Sequoia Research Products (Pangbourne, UK).

Carbon-11 (^{11}C) dioxide was produced by the ^{14}N(p,α)^{11}C nuclear reactions using CYPRIS HM-18 cyclotron (Sumitomo Heavy Industry, Tokyo, Japan). If not otherwise stated, radioactivity was measured with an IGC-3R Curiemeter (Aloka, Tokyo, Japan).

2. Chemistry. The purity of all compounds, radiolabeling precursors **7b**−**12b** and unlabeled **7a**−**12a**, was determined by an analytical HPLC method and was found to be greater than 95% for all compounds (see Supporting Information, Table 1).

*(1R,2S)-2-(((2,4-Dimethylpyrimidin-5-yl)oxy)methyl)-N-(5-fluoro-4-hydroxypyridin-2-yl)-2-(3-fluorophenyl)-cyclopropanecarboxamide (**8b**).* A mixture of **8a** (36 mg, 0.08 mmol) and pyridine hydrochloride was stirred at 120 °C for 2 h. The reaction mixture was allowed to cool to rt, and brine was added to the reaction mixture. The mixture was extracted with ethyl acetate (AcOEt), dried over magnesium sulfate ($MgSO_4$), and evaporated in vacuo. The residue was purified by silica gel column chromatography using *n*-heptane/AcOEt (19/1 to 0/1, v/v) to give **8b** (34.3 mg, 100% yield) as a colorless powder; mp: 132−134 °C. ^{1}H NMR (400 MHz, CD_3OD, δ): 1.59−1.68 (m, 1H), 1.84−1.96 (m, 1H), 2.23 (s, 3H), 2.37−2.45 (m, 1H), 2.49 (s, 3H), 4.38−4.47 (m, 1H), 4.64−4.72 (m, 1H), 6.46−6.67 (brs, 1H), 6.95−7.10 (m, 1H), 7.26−7.45 (m, 3H), 7.69 (d, J = 5.1 Hz, 1H), 8.11 (s, 1H). HRMS (FAB) calcd for $C_{22}H_{20}F_2N_4O_3$, 427.1582; found, 427.1544.

*(1R,2S)-2-(((2-Methyl-4-hydroxymethylpyrimidin-5-yl)oxy)-methyl)-N-(5-fluoropyridin-2-yl)-2-phenylcyclopropanecarboxamide (**12b**).* A solution of bromine (40 μL, 0.76 mmol) in dry $CHCl_3$ (300 uL) was added dropwise to the solution of (1*R*,2*S*)-2-(((2,4-dimethylpyrimidin-5-yl)oxy)methyl)-*N*-(5-fluoropyridin-2-yl)-2-phenyl)cyclopropanecarboxamide (**12c**, 150 mg, 0.38 mmol) in dry $CHCl_3$ (3 mL) at 0 °C and the reaction mixture stirred at rt for 4 days. The reaction mixture was quenched with 1 M sodium thiosulfate and extracted with AcOEt. The organic layer was dried over $MgSO_4$ and evaporated in vacuo. The residue was purified by silica gel column chromatography using *n*-heptane/AcOEt (7/3, v/v) to give (1*R*,2*S*)-2-(((2-methyl-4-bromomethylpyrimidin-5-yl)oxy)methyl)-*N*-(5-fluoropyridin-2-yl)-2-phenylcyclopropanecarboxamide (75 mg, 41.6% yield) as a colorless powder. ^{1}H NMR (300 MHz, $CDCl_3$, δ): 1.64 (dd, J = 5.2, 8.1 Hz, 1H), 1.92 (t, J = 5.2 Hz, 1H), 2.15 (dd, J = 5.2, 8.1 Hz, 1H), 2.58 (s, 3H), 4.24 (s, 2H), 4.56 (s, 2H), 7.30−7.43 (m, 4H), 7.48−7.54 (m, 2H), 8.05−8.12 (m, 1H), 8.12 (d, J = 3.2 Hz, 1H), 8.13 (s, 1H), 8.33 (brs, 1H). HRMS (FAB) calcd for $C_{22}H_{20}BrFN_4O_2$, 471.0832; found, 471.0849.

Sodium acetate (37 mg, 0.45 mmol) was added to the solution of the above-mentioned bromide (70 mg, 0.15 mmol) in DMF (2 mL), and the reaction mixture was heated at 50 °C for 2.5 h. The reaction mixture was partitioned between AcOEt and brine and extracted with AcOEt. The organic layer was dried over $MgSO_4$ and evaporated in vacuo. The residue was dissolved in MeOH (10 mL), and 1 M NaOH (10 mL) was added to the reaction mixture at rt and stirred for 1.5 h. The reaction mixture was partitioned between AcOEt and brine and extracted with AcOEt. The organic layer was dried over $MgSO_4$ and evaporated in vacuo. The residue was purified by silica gel column chromatography using *n*-heptane/AcOEt (4/6, v/v) to give **12b** (49 mg, 81.0% yield) as a colorless amorphous substance. ^{1}H NMR (300 MHz, $CDCl_3$, δ): 1.62 (dd, J = 5.3, 7.9 Hz, 1H), 1.89 (t, J = 5.3 Hz, 1H), 2.13 (dd, J = 5.3, 7.9 Hz, 1H), 2.60 (s, 3H), 3.89 (brs, 1H), 4.43 (d, J = 17.6 Hz, 1H), 4.44 (d, J = 9.5 Hz, 1H), 4.52 (d, J = 9.5 Hz, 1H), 4.53 (d, J = 17.6 Hz, 1H), 7.27−7.47 (m, 6H), 8.02 (s, 1H), 8.07 (dd, J = 3.9, 9.1 Hz, 1H), 8.13 (d, J = 2.9 Hz, 1H), 8.35 (s, 1H). HRMS (FAB) calcd for $C_{22}H_{21}FN_4O_3$, 409.1676; found, 409.1629.

*(1R,2S)-2-(((2-Methyl-4-hydroxymethylpyrimidin-5-yl)oxy)-methyl)-N-(5-fluoropyridin-2-yl)-2-(3-fluorophenyl)-cyclopropanecarboxamide (**9b**).* Compound **9b** was prepared according to the procedure described for the synthesis of **12b** using (1*R*,2*S*)-2-(((2-methyl-4-bromomethylpyrimidin-5-yl)oxy)methyl)-*N*-(5-fluoropyridin-2-yl)-2-(3-fluorophenyl)cyclopropanecarboxamide (100 mg, 0.21 mmol), sodium acetate (60 mg, 0.62 mmol) in DMF (10 mL), and 1 M NaOH (2 mL) in EtOH (10 mL). The product was purified by silica gel column chromatography using *n*-heptane/AcOEt (3/7, v/v) to give **9b** (53 mg, 61% yield) as a colorless powder; mp: 73−75 °C. ^{1}H NMR (600 MHz, CD_3OD, δ): 1.56 (t, J = 6.0 Hz, 1H), 1.85 (t, J = 6.0 Hz, 1H), 2.49 (t, J = 6.0 Hz, 1H), 2.53 (s, 3H), 4.41 (d, J = 12.0 Hz, 1H), 4.49 (d, J = 12.0 Hz, 1H), 4.57 (d, J = 12.0 Hz, 1H), 4.66 (d, J = 12.0 Hz, 1H), 6.98−7.04 (m, 1H), 7.32−7.36 (m, 1H),

dx.doi.org/10.1021/jm400772t | J. Med. Chem. XXXX, XXX, XXX−XXX

7.36−7.39 (m, 2H), 7.44−7.50 (m, 1H), 7.90−7.95 (m, 1H), 8.13 (s, 1H), 8.17 (brs, 1H). ESI-MS: *m/z* 449 (M + Na). HRMS (FAB) calcd for $C_{22}H_{20}F_2N_4O_3$, 427.1582; found, 427.1554.

3. Radiochemistry. All labeled compounds were formulated with sterile saline (3 mL) containing Tween 80 (100 μL) and ascorbic acid (25 mg) after HPLC purification. HPLC analytical and purification conditions for all labeled compounds [^{11}C]**7a**−**12a** are shown in the Supporting Information.

*(1R,2S)-2-(((2,4-Dimethylpyrimidin-5-yl)oxy)methyl)-N-(5-fluoro-6-[^{11}C]methoxypyridin-2-yl)-2-(3-fluorophenyl)-cyclopropanecarboxamide ([^{11}C]**11a**).* [^{11}C]CH_3I was synthesized from cyclotron-produced [^{11}C]CO_2 as described previously.[32] Briefly, [^{11}C]CO_2 was bubbled into 0.04 M $LiAlH_4$ in anhydrous THF (300 μL). After evaporation of THF, the remaining complex was treated with 57% hydroiodic acid (300 μL) to give [^{11}C]CH_3I, which was distilled at 180 °C and transferred under helium gas into a solution of **11b** (1.0 mg, 2.3 μmol) and 0.5 M K_2CO_3 (5 μL, 2.5 μmol) in anhydrous DMF (300 μL) at −15 to −20 °C. After radioactivity reached saturation, this reaction mixture was heated at 50 °C for 3 min. The reaction mixture was applied to a semipreparative HPLC system. HPLC (YMC Pack Pro C_{18}) purification was completed using the mobile phase of MeCN/H_2O/TEA (6/4/0.01, v/v/v) at a flow rate of 5.0 mL/min. The radioactive fraction corresponding to the desire product was collected in a sterile flask, evaporated to dryness in vacuo, redissolved in 3 mL of sterile saline, and passed through a 0.22 μm Millipore filter to give 2.23 GBq of [^{11}C]**11a.** The t_R of [^{11}C]**11a** was 8.8 min for purification and 6.2 min for analysis on HPLC. The specific activity of [^{11}C]**11a** was calculated by comparison of the assayed radioactivity to the mass associated with the carrier UV peak at 254 nm. The synthesis time from end of bombardment (EOB), 31.5 min; radiochemical yield (decay-corrected), 36% based on [^{11}C]CO_2; radiochemical purity, > 99%; specific activity at end of synthesis (EOS), 106 GBq/μmol.

*(1R,2S)-2-(((2,4-Dimethylpyrimidin-5-yl)oxy)methyl)-N-(5-fluoropyridin-2-yl)-2-(3-fluoro-4-[^{11}C]methoxyphenyl)-cyclopropanecarboxamide ([^{11}C]**7a**).* Following the same procedure as that described for [^{11}C]**11a**, [^{11}C]**7a** was obtained from **7b** (1.60 mg, 3.8 μmol). The reaction mixture was purified by HPLC (YMC Pack Pro C_{18}) using the mobile phase of MeOH/H_2O/TEA (7/3/0.01, v/v/v) at a flow rate of 4.0 mL/min to give 1.27 GBq of [^{11}C]**7a**. The t_R of [^{11}C]**7a** was 9.6 min for purification and 5.0 min for analysis on HPLC. The synthesis time from EOB, 28.1 min; radiochemical yield decay-corrected), 28.0% based on [^{11}C]CO_2; radiochemical purity, >99%; specific activity at EOS, 70 GBq/μmol.

*(1R,2S)-2-(((2,4-Dimethylpyrimidin-5-yl)oxy)methyl)-N-(5-fluoro-4-[^{11}C]methoxypyridin-2-yl)-2-(3-fluorophenyl)-cyclopropanecarboxamide ([^{11}C]**8a**).* Following the same procedure as that described for [^{11}C]**11a**, [^{11}C]**8a** was obtained from **8b** (1.33 mg, 3.1 μmol). The reaction mixture was purified by HPLC (YMC Pack Pro C_{18}) using the mobile phase of MeOH/H_2O/TEA (5/5/0.01, v/v/v) at a flow rate of 5.0 mL/min to give 1.05 GBq of [^{11}C]**8a**. The t_R of [^{11}C]**8a** was 9.7 min for purification and 8.4 min for analysis on HPLC. The synthesis time from EOB, 27.5 min; radiochemical yield decay-corrected, 10.7% based on [^{11}C]CO_2; radiochemical purity, >99%; specific activity at EOS, 107 GBq/μmol.

*(1R,2S)-2-(((2-Methyl-4-[^{11}C]methoxymethylpyrimidin-5-yl)oxy)-methyl)-N-(5-fluoropyridin-2-yl)-2-(3-fluorophenyl)-cyclopropanecarboxamide ([^{11}C]**9a**).* [^{11}C]CH_3I was introduced to a solution of **9b** (1.87 mg, 4.4 μmol) and NaH (60% in oil, 600 μg, 15 μmol) in anhydrous DMF (250 μL) at −15 to −20 °C. The reaction mixture was heated at 40 °C for 3 min and purified by HPLC to give [^{11}C]**9a**. The reaction mixture was purified by HPLC (YMC Pack Pro C_{18}) using the mobile phase of MeCN/H_2O/TEA (4.5/5.5/0.01, v/v/v) at a flow rate of 5.0 mL/min to give 1.55 GBq of [^{11}C]**9a**. The t_R of [^{11}C]**9a** was 7.3 min for purification and 11.5 min for analysis on HPLC. The synthesis time from EOB, 33.5 min; radiochemical yield decay-corrected), 21.6% based on [^{11}C]CO_2; radiochemical purity, >99%; specific activity at EOS, 120 GBq/μmol.

*(1R,2S)-2-(((2-Methyl-4-[^{11}C]methoxymethylpyrimidin-5-yl)oxy)-methyl)-N-(5-fluoropyridin-2-yl)-2-phenylcyclopropanecarboxamide ([^{11}C]**12a**).* Following the same procedure as that described for [^{11}C]**9a**, [^{11}C]**12a** was obtained from **12b** (2.40 mg, 5.0 μmol). The reaction mixture was purified by HPLC (YMC Pack Pro C_{18}) using the mobile phase of MeCN/H_2O/TEA (4.5/5.5/0.01, v/v/v) at a flow rate of 5.0 mL/min to give 1.24 GBq of [^{11}C]**12a**. The t_R of [^{11}C]**12a** was 11.3 min for purification and 8.2 min for analysis on HPLC. The synthesis time from EOB, 30.1 min; radiochemical yield decay-corrected, 22.1% based on [^{11}C]CO_2; radiochemical purity, >99%; specific activity at EOS, 101 GBq/μmol.

*(1R,2S)-2-(((2,4-Dimethylpyrimidin-5-yl)oxy)methyl)-N-(5-[^{11}C]-cyanopyridin-2-yl)-2-(3-fluorophenyl)cyclopropanecarboxamide ([^{11}C]**10a**). [^{11}C]HCN Preparation.* [^{11}C]HCN was synthesized by a handmade device in a two-step sequence of reaction. After [^{11}C]CO_2 in N_2 gas from the cyclotron was trapped at −196 °C, it was heated to 50 °C, moved under N_2 stream (flow rate of 10 mL/min), and mixed with H_2 gas at a flow rate of 10 mL/min. The mixed gas was passed through a Ni wire tube at 400 °C in the methanizer to give a mixture of [^{11}C]CH_4 in the carrier gas. Then it was mixed with 5% NH_3 in N_2 (v/v) gas stream at a flow rate of 400 mL/min and passed through Pt furnace at 950 °C to give a [^{11}C]HCN-containing gas, which was absorbed to the reaction solution via a bubbling tube until the radioactivity of the vessel reached saturation (45 s). The average of the total radioactivity recovered in the reaction vessel was about 70% based on [^{11}C]CO_2 at EOS. The synthesis of [^{11}C]**10a** from [^{11}C]HCN via [^{11}C]CuCN was successfully carried out.[35,36]

A freshly prepared solution of sodium metabisulfate (150 μL, 48 mM; 7.2 μmol) was added to a solution of copper(II) sulfate (100 μL, 44 mM; 6.6 μmol) at rt under N_2 stream 10 min prior to EOB. [^{11}C]HCN gas was bubbled into the mixture at rt and a flow rate of 400 mL/min until the radioactivity reached saturation. The solution was then heated to 80 °C for 2 min. A solution of **10b** (3.5 mg, 6.8 μmol) in DMF (250 μL) was added to the reaction mixture at rt and heated to 165 °C for 5 min. The reaction mixture was purified by HPLC (YMC Pack Pro C_{18}) using the mobile phase of MeCN/H_2O/TEA (5/5/0.01, v/v/v) at a flow rate of 5.0 mL/min to give 199.4 MBq of [^{11}C]**10a**. The t_R of [^{11}C]**10a** was 11.0 min for purification and 5.2 min for analysis on HPLC. The synthesis time from EOB, 33.8 min; radiochemical yield (decay-corrected), 2.8% based on [^{11}C]CO_2; radiochemical purity, >99%; specific activity at EOS, 47 GBq/μmol.

4. Receptor Binding Assay for B_{max} Evaluation. *Preparation of Brain Homogenate.* Parts of the cerebral cortex which contained mainly layer VI were collected from Sprague−Dawley (SD) rats (male, 7 weeks old, *n* = 11, Charles River, Yokohama, Japan). Wet cerebral cortex tissues were weighed, homogenized in 0.32 M sucrose and 10 mM Tris-HCl (pH 8.0) on ice, and centrifuged (1000*g*, 4 °C, 10 min). The supernatant was collected and centrifuged (30 000*g*, 4 °C, 20 min). The precipitate was suspended in 1 mM ethylene glycol bis(2-aminoethyl ether)-*N,N,N′,N′*-tetraacetic acid (EGTA) and 50 mM Tris-HCl (pH 8.0) on ice and centrifuged (30 000*g*, 4 °C, 20 min); this procedure was conducted two times. Next the precipitate was suspended in 2 mM EGTA, 10 mM $MgCl_2$, and 20 mM 4-(2-hydroxyethyl)-1-piperazinethanesulfonic acid (HEPES, pH 7.4) on ice and centrifuged (30 000*g*, 4 °C, 20 min); this procedure was repeated three times. The precipitate was suspended in 2 mM EGTA, 10 mM $MgCl_2$, and 20 mM HEPES (pH 7.4). This microsomal fraction was stored as a receptor stock solution at −80 °C until use.

Binding Assay. Receptor stock solution was resuspended in binding buffer (1 mM $CaCl_2$, 5 mM $MgCl_2$, and 25 mM HEPES, pH 7.4) to a final concentration of 5 mg tissue equiv/assay. The incubation time for [^{3}H]**4** on OX_2R was 60 min at 25 °C. After incubation, membranes were filtered onto a GF/B filter and washed three times with ice−cold wash buffer (same as the binding buffer). Each filter was placed in a vial and 5 mL of liquid scintillator reagent (Atomlight; PerkinElmer Life & Analytical Sciences) were added. Radioactivity was counted (2 min) in a liquid scintillation counter (2500, PerkinElmer Life & Analytical Sciences).

Saturation isotherms were determined by addition of various concentrations of [^{3}H]**4** (5−1280 nM). Nonspecific binding for [^{3}H]**4** was measured in the presence of 0.1 mM unlabeled **4**. B_{max} was calculated by Scatchard analysis of the saturation isotherm experiment.

dx.doi.org/10.1021/jm400772t | J. Med. Chem. XXXX, XXX, XXX−XXX

5. Measurement of Lipophilicity. cLogP values of tested compounds were determined computationally using Daylight Software ver. 4.94 (Daylight Chemical Information Systems, Inc., Niguel, CA). log *D* values of selected compounds were measured by mixing ^{11}C-labeled compound (radiochemical purity, 100%; about 200 000 cpm) with *n*-octanol (3.0 g) and phosphate-buffered saline (PBS; 3.0 g, 0.1 M, pH 7.4) in a test tube. The mixture was vortexed for 3 min at rt, followed by centrifugation at 2330*g* for 5 min. Aliquots of 1 mL of PBS and 1 mL of *n*-octanol were removed and weighed, and their radioactivity was quantified with a 1480 Wizard automatic γ counter (Perkin-Elmer, Waltham, MA). Sample from the remaining organic layer was removed and repartitioned until a consistent log *D* was obtained. The log *D* value was calculated by the following formula: log *D* = log[(cpm/g *n*-octanol)/(cpm/g PBS)]. All measurements were performed in triplicate.

6. P-gp Transcellular Transport Study.[26,37] LLC-PK1 and LLC-MDR1 cells were seeded at a density of 4.0×10^5 cells/cm^2 onto porous membrane filters of 24-well cell culture insert plates. Cells were cultured in 5% CO_2 at 37 °C and were used for the transport studies 5 days after seeding. For transcellular transport experiments, each cell monolayer was preincubated at 37 °C for 2 h in Hank's balanced salt solution containing 10 mM HEPES (HBSS buffer).

Transcellular transport experiments were initiated by adding the solution of test compounds to the apical or basal side of the cell culture inserts. After incubation at 37 °C for 2 h, HBSS buffer was sampled from the compartment opposite to that spiked with test compounds and was analyzed for test compound concentration by LC-MS. The apparent permeability coefficient (P_{app}) of the test compounds were estimated using eq 1, where Q, t, C_0, and A represent permeated amount of test compounds, incubation time, initial concentration of test compounds, and membrane area, respectively.

$$P_{app} = Q/t/C_0/A \quad (1)$$

Both FRs across the monolayer, LLC-PK1 and LLC-MDR1, were defined according to eq 2, where $P_{app,\ b\ to\ a}$ and $P_{app,\ a\ to\ b}$ represent the P_{app} in the basal-to-apical direction and the apical-to-basal, and the corrected FR was defined by eq 3.

$$\mathrm{FR} = P_{app,btoa}/P_{app,atob} \quad (2)$$

$$\text{corrected FR} = (\text{FR in LLC-MDR1cells})/(\text{FR in LLC-PK1cells}) \quad (3)$$

7. Animals. SD rats at 9−11 weeks of age (male, 410−500 g) were purchased from Japan SLC (Shizuoka, Japan), and P-gp-knockout rats at 10 weeks of age (Mdr1a knockout rats, male, 410−500 g) were purchased from SAGE Laboratories (St. Louis, MO). The animals were housed under a 12 h light−dark cycle, allowed free access to food pellets and water, and used for in vivo PET studies. A rhesus monkey at 3 years and 8 months of age (male, 4.25 kg) was purchased from Japan SLC (Shizuoka, Japan). The monkey was housed in an individual cage and was supplied with a balanced diet and ad libitum tap water from a feeding valve. The room was illuminated from 7 a.m. to 9 p.m. Age and body weight of the monkey at that time of PET scan was 3 years and 11 months and 4.65 kg, respectively. The animal experiments were approved by the Animal Ethics Committee of National Institute of Radiological Sciences (NIRS).

8. In Vitro Binding Assays for K_i Value Evaluation. Human OX_1R- or OX_2R-expressing CHO cells (Chinese hamster ovary cells) were homogenized in 20 mM HEPES buffer (pH = 7.4) containing 10 mM $MgCl_2$ and 2 mM EGTA with a Polytron homogenizer (Kinematica AG, Lucerne, Switzerland). The homogenate was centrifuged at 1000*g* for 10 min at 4 °C, and the supernatant was further centrifuged at 40 000*g* for 45 min at 4 °C (Beckman Coulter, Fullerton, CA). The pellet was resuspended in the same buffer and stored at −80 °C before use.

Cell homogenate was diluted to 250 μg/mL in 25 mM HEPES buffer (pH = 7.5) containing 5 mM $MgCl_2$, 1 mM $CaCl_2$, 0.5% BSA, 0.1% sodium azide, and 0.05% Tween 20. Twenty microliters of membrane suspension of OX_1R or OX_2R containing 5 μg protein was mixed with 10 μL of compounds, Orexin A (100 μM, Peptide Institute, Osaka, Japan) solution or vehicle and 10 μL of [^{125}I]-orexin A solution (2 nM, PerkinElmer, Waltham, MA) and 60 μL of assay buffer (final volume: 100 μL) and the mixture incubated for 30 min at rt on a 96-well Flashplate (PerkinElmer). All reaction mixtures were discarded and washed with 200 μL of 25 mM HEPES buffer containing 525 mM of NaCl. The radioactivity (disintegrations per minute, DPM) of each well was measured using a TopCount device (PerkinElmer). The inhibitory activities of test compounds were calculated using the following formula:

$$\text{inhibition \%} = 100 - 100 \times (T - \mathrm{N})/(C - N)$$

T: DPM in the presence of compounds (test)

N: 10 μM orexin A (nonspecific binding)

C: DPM in the absence of compound (control)

All values were determined as averages of three wells in a single measurement.

9. In Vitro Autoradiography. *For Screening.* Rat brain sections (20 μm thick) were dried at rt and preincubated for 20 min in 25 mM HEPES buffer (pH 7.4) containing 5 mM $MgCl_2$ and 1 mM $CaCl_2$ at rt. After preincubation, these sections were incubated for 60 min at rt in fresh buffer with [^{11}C]**7a** (7.6 nM), [^{11}C]**8a** (2.0 nM), [^{11}C]**9a** (2.5 nM), [^{11}C]**10a** (59.0 nM), [^{11}C]**11a** (1.6 nM), [^{11}C]**12a** (2.6 nM), respectively. Unlabeled compounds **7a**−**12a** (10 μM) were used to assess the nonspecific binding of these radioligands in the brain. After incubation, brain sections were rapidly washed with cold distilled water three times and dried at rt. An imaging plate (BAS-IP MS2025, Fujifilm, Tokyo, Japan) was exposed to the dried sections for 1 h. Radioactive standards calibrated with known amounts of [^{11}C]**7a**−[^{11}C]**12a** were induced in the exposure process. Quantitative autoradiogram analysis was performed using a computer-assisted image analyzer (Multi Gauge; Fujifilm). Optical density values were converted to fmol/mg protein using a computer-generated regression analysis which compared film densities produced by tissue sections and radioactive standards.

*Assessment of Specificity of **9a** for OXRs.* All procedures were performed as in the above-mentioned screening method. [^{11}C]**9a** (3.6 nM) and unlabeled compounds **3** (20 μM) and **4** (200 nM) were used. Coronal slices were collected at +1.5 mm and −3.0 mm to bregma. Representative autoradiograms were acquired from serial brain sections, and the neocortical layer VI in each slice was encircled based on the brain atlas. Radioactivity in this area was then measured in eight slices (consisting of two slices generated at +1.5 mm to bregma and six slices at −3.0 mm to bregma, n = 3).

10. Animal PET Studies. *Wild-Type Rats.* Prior to PET scans, anatomical template images of the rat brain were generated by a high-resolution MRI system. Briefly, a rat was anesthetized with sodium pentobarbital (50 mg/kg, ip) and scanned with a 400 mm bore, 7 T horizontal magnet (NIRS/KOBELCO, Kobe, Japan/Bruker BioSpin) equipped with 120 mm diameter gradients (Bruker BioSpin). A 72 mm diameter coil was used for radiofrequency transmission, and signals were received by a four-channel surface coil. Coronal T2-weighted MRI images were obtained by a fast spin−echo sequence with the following imaging parameters: repetition time = 8000 ms, effective echo time = 15 ms, field of view (FOV) = 35 mm × 35 mm, and slice thickness = 0.6 mm.

PET scans for anesthetized SD rats (male, 410−500 g) were performed with a small animal-dedicated micro PET FOCUS 220 system (Siemens Medical Solutions, Malvern, PA), which yields a 25.8 cm (transaxial) × 7.6 cm (axial) FOV, and a spatial resolution of 1.3 mm full-width at half-maximum (fwhm) at the center of FOV.[38] Subsequently, list-mode scans were performed for 90 min. All list-mode data were sorted and Fourier-rebinned into two-dimensional sinograms (frames, 1 min × 4 scans, 2 min × 8 scans, 5 min × 14 scans). Images were thereafter reconstructed using two-dimensional filtered back-projection with a 0.5-mm Hanning filter. To inject [^{11}C]**9a**, a 24-gauge needle with catheter (Terumo, Tokyo, Japan) was

dx.doi.org/10.1021/jm400772t | J. Med. Chem. XXXX, XXX, XXX−XXX

placed into the rat tail vein. The injected dose of the radioligand was 78.7−189.8 MBq (127.6 ± 43.1 MBq, mean ± SD). Body temperature was maintained with a 37 °C plate heater (Bio Research Center Inc., Aichi, Japan). During the scan, the rat was maintained under anesthesia with 1.5% (v/v) isoflurane. For the inhibition study, unlabeled **9a** (10 mg/kg, po, dissolved **9a** with 5% DMSO and 10% cremophore in 10 mM HCl, in H_2O) was administered to the rat 1 h before the radioligand injection.

P-gp-knockout Rats. PET scans for P-gp-knockout rats (male, 410−500 g) were performed in the same manner as in the scans for SD rats.

Rhesus Monkey. MRI images of the monkey brain were generated by an apparatus identical to that for the above-mentioned rat MRI. Horizontal brain MRI images were obtained by a gradient echo pulse sequence termed FLASH with the following imaging parameters: repetition time = 481 ms, effective echo time = 7.6 ms, FOV = 110 mm × 110 mm, slice thickness = 1.5 mm. PET scans for a monkey was performed using a high-resolution SHR-7700 PET camera (Hamamatsu Photonics, Shizuoka, Japan) designed for laboratory animals, which provides 31 transaxial slices 3.6 mm (center-to-center) apart and a 33.1 cm (transaxial) × 11.16 cm (axial) FOV. The spatial resolution for the reconstructed images was 2.6 mm fwhm at the center of FOV.[39] Prior to PET scans, the monkey was initially anesthetized with thiamylal, and anesthesia was maintained using 1.5% (v/v) isoflurane. Following a transmission scan for attenuation correction using a ^{68}Ge-^{68}Ga source, dynamic emission scans were conducted in a three-dimensional acquisition mode for 90 min (frames, 1 min × 4 scans, 2 min × 8 scans, 5 min × 14 scans). Emission scan images were reconstructed with a 4 mm Colsher filter. [^{11}C]**9a** was injected via the crural vein as a single bolus at the start of emission scanning. Injected dose of the radioligand was 115.5 MBq. An additional PET measurement was carried out by injecting a P-gp inhibitor, tariquidar (8 mg/kg/5 mL of saline with 10% DMSO), via the crural vein as a single slow bolus over 10 min at 0.25 h before [^{11}C]**9a** administration. Injected dose of the radioligand was 87.7 MBq. All PET scans were acquired in the same monkey.

Image Acquisition and Data Analysis. Anatomical regions of interest (ROIs) were manually defined on the striatum, thalamus, pons, and cerebellum in the PET images coregistered with MRI images using PMOD software (PMOD Technologies Ltd., Zurich, Switzerland). Regional radioactivity in the brain was decay-corrected to the injection time and was expressed as the percent of injected dose (% ID/mL = % injected dose/cm^3 brain) in rat experiments and as the percentage standardized uptake value [% SUV = % ID/mL × body weight (g)] in monkey experiments.

11. Metabolite Study for Rat Plasma and Brain. After the intravenous injection of [^{11}C]**9a** (330 MBq/0.1 mL), a P-gp-knockout rat (male Mdr1a-knockout rat weighing 450 g, identical to one of the individuals used for the PET imaging, male) was killed by decapitation at 30 min. Blood and whole brain were quickly removed, and the blood sample (0.5 mL) was centrifuged at 20 000*g* for 2 min.at 4 °C to separate plasma. The supernatant (0.2 mL) was then collected in a test tube containing MeCN (0.2 mL), and resulting mixture was vortexed for 15 s and centrifuged at 20 000*g* for deproteinization. The resulting supernatant was collected. Subsequently, the one-half of a rat brain was homogenized with a Silent Crusher S homogenizer (Rose Scientific Ltd., Edmonton, Canada) in ice-cold 50% aqueous MeCN (2.5 mL) solution. The resulting homogenate was centrifuged at 20 000*g* for 2 min at 4 °C. The supernatant (0.5 mL) was collected and resuspended with an equal volume of MeCN (0.5 mL) followed by centrifugation at 20 000*g* for 2 min for deproteinization. Supernatants (500 μL) were analyzed by HPLC (Capcell Pak C_{18}, S-5 μm, 4.6 mm ID × 250 mm, Shiseido, Tokyo, Japan) combined to analytical radio-UPLC using the mobile phase of MeCN/H_2O/TEA (5/5/0.01, v/v/v) at a flow rate of 1.5 mL/min. Fraction of unmetabolized [^{11}C]**9a** as the percentage of total radioactivity (decay corrected) in the HPLC chromatogram was calculated as: (peak area for [^{11}C]**9a**/total peak area) × 100.

12. GPCR Panel Assay. Target GPCRs were stably expressed in human embryonic kidney (HEK) 293 cells, a subset of which coexpressed Gqi5 chimeric G-protein (Gqi5/HEK293), to convert its Gi signaling to Ca^{2+} response.[40] Thereafter, GPCRs+Gqi5/HEK293 and Gqi5/HEK293 cells were seeded separately at 5000/25 μL/well into collagen type I-coated 384-well plates and cultured overnight in Dulbecco's Modified Eagle's Medium. Subsequently, calcium-sensitive fluorescent dye was added to cells and incubated for 1 h at 37 °C.

Measurement of Agonistic Activity. For quantification of agonistic activity, **9a** was added to cells and calcium response was recorded. Solutions of agonistic reference ligands were diluted in wells of cell plates with equal volumes (25 μL) of cell culture medium, calcium dye, and assay buffer. Solutions of **9a** were diluted in wells of cell plates wells with equal volumes (25 μL each) of cell culture medium and calcium dye, resulting in final concentrations of 3, 10, and 30 μM, respectively.

Measurement of Antagonistic Activity against Low or High Dose of Agonistic Reference Ligand. For quantification of antagonistic activity, solutions of **9a** were diluted in wells of cell plates with equal volumes (25 μL each) of cell culture medium, calcium dye, and an excess concentration of agonistic reference ligands resulting in final concentrations of 3, 10, and 30 μM for **9a**. Cells were first incubated with **9a** for 1 h at rt, and then reference ligands at a dose inducing either 20% (EC_{20}) or 80% (EC_{80}) of maximal response were added to detect inhibitory effects of **9a** against these reference ligands. Ca^{2+} concentration was visualized in real time using a calcium indicator dye (Calcium 4, Molecular Devices, Sunnyvale, CA), and fluorescence was detected by the FDSS7000 device (Hamamatsu Photonics, Hamamatsu, Japan).

■ ASSOCIATED CONTENT

Ⓢ Supporting Information

Purities of **7a−12a** and precursors **7b−12b** determined by HPLC. Spectrum data for **7a−12a** and precursors **7b−12b**. HPLC analytic charts for **7a−12a** and precursors **7b−12b**;. HPLC purification charts for [^{11}C]**7a**−[^{11}C]**12a**. HPLC analytical charts for [^{11}C]**7a**−[^{11}C]**12a**. GPCR panel assays to determine off-target activity of 10 μM of **9a**. Rat PET study of [^{11}C]**8a**. This material is available free of charge via the Internet at http://pubs.acs.org.

■ AUTHOR INFORMATION

Corresponding Author

*Phone: +81 43 206 4700. Fax: +81 43 253 0396. E-mail: mhiguchi@nirs.go.jp.

Notes

The authors declare no competing financial interest.

■ ACKNOWLEDGMENTS

The authors are grateful to the staff of NIRS and Eisai for support with the cyclotron operation, radioisotope production, radiosynthesis, and animal experiments, Mr. Yuichiro Yoshida, Masanao Ogawa, and Nobuki Nengaki for manipulating the semiautosynthetic machine in the hot cell, Dr. Masayuki Fujinaga for log *D* measurement, Mr. Takashi Ueno for the P-gp assay, Dr. Carsten Beuckmann for pharmacological support, Mr. Kenji Furutsuka for HRMS, Dr. Yuji Nagai for monkey PET scans, Ms. Kaori Yamada for rat PET scans, Dr. Toru Arai for the GPCR panel assay, Mr. Tomoteru Yamasaki for radiometabolite analysis, and Dr. Francois Bernier, Dr. Krause Stephen, and Dr. Paul McCracken for their assistance in the preparation of the manuscript.

■ ABBREVIATIONS USED

AUC, area under time−activity curve; BBB, blood−brain barrier; B_{max}, the maximum binding; CER, cerebellum; CHO cells, Chinese hamster ovary cells; CNS, central nervous system; CTX, neocortex; DCM, dichloromethane; DIAD,

diisopropyl azodicarboxylate; DIPEA, *N,N*-diisopropylethylamine; DMF, *N,N*-dimethylformamide; DMSO, dimethyl sulfoxide; DPM, disintegrations per minute; EGTA, ethylene glycol bis(2-aminoethylether)-*N,N,N′,N′*-tetraacetic acid; EOB, end of bombardment; EOS, end of synthesis; ESI-MS, electrospray ionization mass spectra; FAB-MS, fast atom bombardment mass spectra; FOV, field of view; FR, flux ratio; fwhm, full-width at half-maximum; GPCR, G-protein-coupled receptor; HATU, *N,N,N′,N′*-tetramethyl-*O*-(7-azabenzotriazol-1-yl)uronium hexafluorophosphate; HEPES, 4-(2-hydroxyethyl)-1-piperazinethanesulfonic acid; HIP, hippocampus; HOBt, 1-hydroxybenzotriazole monohydrate; HPLC, high-performance liquid chromatography; HRMS, high-resolution mass spectra; % ID/mL, percentage of injected radioligand dose per unit volume of tissue; K_d, dissociation constant; K_i, inhibition constant; MDR1, multidrug resistance protein 1; MOM, methoxymethyl; MPFC, medial prefrontal cortex; MRI, magnetic resonance imaging; NaHMDS, sodium hexamethyldisilazane; OXR, orexin receptor; OX_1R, orexin-1 receptor; OX_2R, orexin-2 receptor; PBS, phosphate-buffered saline; PET, positron emission tomography; $Pd_2(dba)_3$, tris(dibenzylideneacetone)dipalladium(0); P-gp, P-glycoprotein; ROI, regions of interest; rt, room temperature; SD, standard deviation; TEA, triethylamine; THA, thalamus; THF, tetrahydrofuran; t_R, retention time; WSC, 1-ethyl-3-(3-dimethylaminopropyl)carbodiimide hydrochloride; Xant phos, 4,5-bis(diphenylphosphino)-9,9-dimethylxanthene

REFERENCES

(1) Sakurai, T.; Amemiya, A.; Ishii, M.; Matsuzaki, I.; Chemelli, R. M.; Tanaka, H.; Williams, S. C.; Richardson, J. A.; Kozlowski, G. P.; Wilson, S.; Arch, J. R. S.; Buckingham, R. E. C.; Haynes, A. C.; Carr, S. A.; Annan, R. S.; McNulty, D. E.; Liu, W.-S.; Terrett, J. A.; Elshourbagy, N. A.; Bergsma, D. J.; Yanagisawa, M. Orexins and orexin receptors: A family of hypothalamic neuropeptides and G protein-coupled receptors that regulate feeding behavior. *Cell* **1998**, *92*, 573−585.

(2) van den Pol, A. N.; Gao, X.-B.; Obrietan, K.; Kilduff, T. S.; Belousov, A. B. Presynaptic and postsynaptic actions and modulation of neuroendocrine neurons by a new hypothalamic peptide, hypocretin/orexin. *J. Neurosci.* **1998**, *18*, 7962−7971.

(3) Brisbare-Roch, C.; Dingemanse, J.; Koberstein, R.; Hoever, P.; Aissaoui, H.; Flores, S.; Mueller, C.; Nayler, O.; van Gerven, J.; de Haas, S. L.; Hess, P.; Qiu, C.; Buchmann, S.; Scherz, M.; Weller, T.; Fischli, W.; Clozel, M.; Jenck, F. Promotion of sleep by targeting the orexin system in rats, dogs and humans. *Nat. Med.* **2007**, *13*, 150−155.

(4) Thompson, J. L.; Borgland, S. L. A role for hypocretin/orexin in motivation. *Behav. Brain Res.* **2011**, *217*, 446−453.

(5) Nishino, S. Chapter 47 - Hypothalamus, hypocretins/orexin, and vigilance control. *Handb. Clin. Neurol.* **2011**, *99*, 765−782.

(6) Zhang, J.; Li, B.; Yu, L.; He, Y.-C.; Li, H.-Z.; Zhu, J.-N.; Wang, J.-J. A role for orexin in central vestibular motor control. *Neuron* **2011**, *69*, 793−804.

(7) Okumura, T.; Nozu, T. Role of brain orexin in the pathophysiology of functional gastrointestinal disorders. *J. Gastroenterol. Hepatol.* **2011**, *26*, 61−66.

(8) Sakurai, T. Orexins and orexin receptors: implication in feeding behavior. *Regul. Pept.* **1999**, *85*, 25−30.

(9) Sharf, R.; Sarhan, M.; Dileone, R. J. Role of orexin/hypocretin in dependence and addiction. *Brain Res.* **2010**, *1314*, 130−138.

(10) Coleman, P. J.; Renger, J. J. Orexin receptor antagonists: a review of promising compounds patented since 2006. *Expert. Opin. Ther. Pat.* **2010**, *20*, 307−324.

(11) Bingham, M. J.; Cai, J.; Deehan, M. R. Eating, sleeping and rewarding: orexin receptors and their antagonists. *Curr. Opin. Drug. Discovery Dev.* **2006**, *9*, 551−559.

(12) Boss, C.; Brisbare-Roch, C.; Jenck, F. Biomedical application of orexin/hypocretin receptor ligands in neuroscience. *J. Med. Chem.* **2009**, *52*, 891−903.

(13) Cai, J.; Cooke, F. E.; Sherborne, B. S. Antagonists of the orexin receptors. *Curr. Opin. Drug. Discovery Dev.* **2006**, *16*, 631−646.

(14) Roecker, A. J.; Coleman, P. J. Orexin receptor antagonists: medicinal chemistry and therapeutic potential. *Curr. Top. Med. Chem.* **2008**, *8*, 977−987.

(15) Gatfield, J.; Brisbare-Roch, C.; Jenck, F.; Boss, C. Orexin receptor antagonists: a new concept in CNS disorders? *Chem. Med. Chem.* **2010**, *5*, 1197−1214.

(16) Winrow, C. J.; Gotter, A. L.; Cox, C. D.; Doran, S. M.; Tannenbaum, P. L.; Breslin, M. J.; Garson, S. L.; Fox, S. V.; Harrell, C. M.; Stevens, J.; Reiss, D. R.; Cui, D.; Coleman, P. J.; Renger, J. J. Promotion of sleep by suvorexant - a novel dual orexin receptor antagonist. *J. Neurogenet.* **2011**, *25*, 52−61.

(17) Malherbe, P.; Borroni, E.; Pinard, E.; Wettstein, J. G.; Knoflach, F. Biochemical and electrophysiological characterization of almorexant, a dual orexin 1 receptor (OX1)/orexin 2 receptor (OX2) antagonist: comparison with selective OX1 and OX2 antagonists. *Mol. Pharmacol.* **2009**, *76*, 618−31.

(18) Malherbe, P.; Borroni, E.; Gobbi, L.; Knust, H.; Nettekoven, M.; Pinard, E.; Roche, O.; Rogers-Evans, M.; Wettstein, J. G.; Moreau, J. L. Biochemical and behavioural characterization of EMPA, a novel high-affinity, selective antagonist for the OX(2) receptor. *Br. J. Pharmacol.* **2009**, *156*, 1326−1341.

(19) Langmead, C. J.; Jerman, J. C.; Brough, S. J.; Scott, C.; Porter, R. A.; Herdon, H. J. Characterisation of the binding of [^{3}H]-SB-674042, a novel nonpeptide antagonist, to the human orexin-1 receptor. *Br. J. Pharmacol.* **2004**, *141*, 340−346.

(20) Liu, F.; Majo, V. J.; Prabhakaran, J.; Castrillion, J.; Mann, J. J.; Martinez, D.; Kumar, J. S. D. Radiosynthesis of [^{11}C]BBAC and [^{11}C]BBPC as potential PET tracers for orexin2 receptors. *Bioorg. Med. Chem. Lett.* **2012**, *22*, 2172−2174.

(21) Wang, C.; Moseley, C. K.; Carlin, S. M.; Wilson, C. M.; Neelamegam, R.; Hooker, J. M. Radiosynthesis and evaluation of [^{11}C]EMPA as a potential PET tracer for orexin 2 receptors. *Bioorg. Med. Chem.* **2013**, *23*, 3389−3392.

(22) Trivedi, P.; Yu, H.; MacNeil, D. J.; Van der Ploeg, L. H. T.; Guan, X. -M. Distribution of orexin receptor mRNA in the rat brain. *FEBS Lett.* **1998**, *438*, 71−75.

(23) Marcus, J. N.; Aschkenasi, C. J.; Lee, C. E.; Chemelli, R. M.; Saper, C. B.; Yanagisawa, M.; Elmquist, J. K. Differential expression of orexin receptors 1 and 2 in the rat brain. *J. Comp. Neurol.* **2001**, *435*, 6−25.

(24) Wright, G. J.; Cherwinski, H.; Foster-Cuevas, M.; Brooke, G.; Puklavec, M. J.; Bigler, M.; Song, Y.; Jenmalm, M.; Gorman, D.; McClanahan, T.; Liu, M. R.; Brown, M. H.; Sedgwick, J. D.; Phillips, J. H.; Barclay, A. N. Characterization of the CD200 receptor family in mice and humans and their interactions with CD200. *J. Immunol.* **2003**, *171*, 3034−3046.

(25) Terauchi, T.; Takemura, A.; Doko, T.; Yoshida, Y.; Tanaka, T.; Sorimachi, K.; Naoe, Y.; Beuckmann, C.; Kazuta, Y. Cyclopropane compound. WO 2012/039371 A1, 2010.

(26) Adachi, Y.; Suzuki, H.; Sugiyama, Y. Comparative studies on in vitro methods for evaluating in vivo function of MDR1 P-glycoprotein. *Pharm. Res.* **2001**, *18*, 1660−1668.

(27) Mintun, M. A.; Raichle, M. E.; Kilbourn, M. R.; Wooten, G. F.; Welch, M. J. A quantitative model for the in vivo assessment of drug binding sites with positron emission tomography. *Ann. Neurol.* **1984**, *15*, 217−227.

(28) Eckelman, W. C.; Mathis, C. A. Targeting proteins in vivo: in vitro guidelines. *Nucl. Med. Biol.* **2006**, *33*, 161−164.

(29) Eckelman, W. C.; Kilbourn, M. R.; Mathis, C. A. Discussion of targeting proteins in vivo: In vitro guidelines. *Nucl. Med. Biol.* **2006**, *33*, 449−451.

(30) Guo, Q.; Brady, M.; Gunn, R. N. A biomathematical modeling approach to central nervous system radioligand discovery and development. *J. Nucl. Med.* **2009**, *50*, 1715−1723.

(31) Kazuta, Y.; Tsujita, R.; Yamashita, K.; Uchino, S.; Kohsaka, S.; Matsuda, A.; Shuto, S. Synthesis of derivatives of (1*S*,2*R*)-1-phenyl-2-[(*S*)-1- aminopropyl]-*N*,*N*-diethylcyclopropanecarboxamide (PPDC) modified at the 1-aromatic moiety as novel NMDA receptor antagonists: The aromatic group is essential for the activity. *Bioorg. Med. Chem.* **2002**, *10*, 3829−3848.
(32) Suzuki, K.; Inoue, O.; Hashimoto, K.; Yamasaki, T.; Kuchiki, M.; Tamate, K. Computer-controlled large scale production of high specific activity [^{11}C]RO 15-1788 for PET studies of benzodiazepine receptors. *Int. J. Appl. Radiat. Isot.* **1985**, *36*, 971−976.
(33) Batailler, M.; Mullier, A.; Sidibe, A.; Delagrange, P.; Prévot, V.; Jockers, R.; Migaud, M. Neuroanataomical distribution of the orphan GPR50 receptor in adult sheep and rodent brains. *J. Neuroendocrinol.* **2011**, *23*, 1365−2826.
(34) Yasuno, F.; Zoghbi, S. S.; Mccarron, J. A.; Hong, J.; Ichise, M.; Brown, A. K.; Gladding, R. L.; Bacher, J. D.; Pike, V. W.; Innis, R. B. Quantification of serotonin 5-HT$_{1A}$ receptors in monkey brain with [^{11}C](*R*)-(−)-RWAY. *Synapse* **2006**, *60*, 510−520.
(35) Iwata, R.; Ido, T.; Takahashi, T.; Nakanishi, H.; Iida, S. Optimization of [^{11}C]HCN production and no-carrier-added [1-^{11}C]amino acid synthesis. *Int. J. Radiat. Appl. Instrum. A* **1987**, *38*, 97−102.
(36) Mathews, W. B.; Monn, J. A.; Ravert, H. T.; Holt, D. P.; Schoepp, D. D.; Dannals, R. F. Synthesis of a mGluR5 antagonist using [^{11}C]copper(I) cyanide. *J. Labelled Compd. Radiopharm.* **2006**, *49*, 829−834.
(37) Sugimoto, H.; Matsumoto, S.; Tachibana, M.; Niwa, S.; Hirabayashi, H.; Amano, N.; Moriwaki, T. Establishment of in vitro P-glycoprotein inhibition assay and its exclusion criteria to assess the risk of drug−drug interaction at the drug discovery stage. *J. Pharm. Sci.* **2011**, *100*, 4013−4023.
(38) Tai, Y. C.; Ruangma, A.; Rowland, D.; Siegel, S.; Newport, D. F.; Chow, P. L.; Laforest, R. Performance evaluation of the microPET focus: A third-generation microPET scanner dedicated to animal imaging. *J. Nucl. Med.* **2005**, *46*, 455−463.
(39) Watanabe, M.; Okada, H.; Shimizu, K.; Omura, T.; Yoshikawa, E.; Kosugi, T.; Mori, S.; Yamashita, T. A high resolution animal PET scanner using compact PS-PMT detectors. *IEEE Trans. Nucl. Sci.* **1997**, *44*, 1277−1282.
(40) Coward, P.; Wada, H. G.; Falk, M. S.; Chan, S. D.; Meng, F.; Akil, H.; Conklin, B. R. Controlling signaling with a specifically designed G$_i$-coupled receptor. *Proc. Natl. Acad. Sci. U.S.A.* **1998**, *95*, 352−357.